Far field tsunami simulations of the 1755 Lisbon earthquake: Implications for tsunami hazard to the U.S. East Coast and the Caribbean

Roy Barkan[a], Uri ten Brink[b,*], Jian Lin[c]

[a] *Department of Geophysics and Planetary Sciences, Tel Aviv University, Ramat Aviv, Tel-Aviv 69978, Israel*

[b] *U.S. Geological Survey, Woods Hole, MA 02543, USA*

[c] *Department of Geology and Geophysics, Woods Hole Oceanographic Institution, Woods Hole, MA 02543, USA*

---

* Corresponding author: Uri ten Brink, USGS Woods Hole Science Center, 384 Woods Hole Rd., Woods Hole, MA 02543 USA. Tel: +1-508-457-2396 ; Fax: +1-508-457-2310 *E-mail address:* utenbrink@usgs.gov

Abstract

The great Lisbon earthquake of November 1st, 1755 with an estimated moment magnitude of 8.5-9.0 was the most destructive earthquake in European history. The associated tsunami run-up was reported to have reached 5-15 m along the Portuguese and Moroccan coasts and the run-up was significant at the Azores and Madeira Island. Run-up reports from a trans-oceanic tsunami were documented in the Caribbean, Brazil and Newfoundland (Canada). No reports were documented along the U.S. East Coast. Many attempts have been made to characterize the 1755 Lisbon earthquake source using geophysical surveys and modeling the near-field earthquake intensity and tsunami effects. Studying far field effects, as presented in this paper, is advantageous in establishing constraints on source location and strike orientation because trans-oceanic tsunamis are less influenced by near source bathymetry and are unaffected by triggered submarine landslides at the source. Source location, fault orientation and bathymetry are the main elements governing transatlantic tsunami propagation to sites along the U.S. East Coast, much more than distance from the source and continental shelf width. Results of our far and near-field tsunami simulations based on relative amplitude comparison

limit the earthquake source area to a region located south of the Gorringe Bank in the center of the Horseshoe Plain. This is in contrast with previously suggested sources such as Marqués de Pombal Fault, and Gulf of Cádiz Fault, which are farther east of the Horseshoe Plain. The earthquake was likely to be a thrust event on a fault striking ~345° and dipping to the ENE as opposed to the suggested earthquake source of the Gorringe Bank Fault, which trends NE-SW. Gorringe Bank, the Madeira-Tore Rise (MTR), and the Azores appear to have acted as topographic scatterers for tsunami energy, shielding most of the U.S. East Coast from the 1755 Lisbon tsunami. Additional simulations to assess tsunami hazard to the U.S. East Coast from possible future earthquakes along the Azores-Iberia plate boundary indicate that sources west of the MTR and in the Gulf of Cadiz may affect the southeastern coast of the U.S. The Azores-Iberia plate boundary west of the MTR is characterized by strike-slip faults, not thrusts, but the Gulf of Cadiz may have thrust faults. Southern Florida seems to be at risk from sources located east of MTR and South of the Gorringe Bank, but it is mostly shielded by the Bahamas. The Gulf of Cádiz is another source area of potential tsunami hazard to the U.S. East Coast. Higher resolution near-shore bathymetry along the U.S. East Coast and the Caribbean as well as a detailed study of potential tsunami sources in the central west part of the Horseshoe Plain are necessary to verify our simulation results.

Keywords: tsunami modeling, 1755 Lisbon earthquake, Azores-Gibraltar plate boundary, U.S. East Coast, Caribbean tsunami

---

1. Introduction

The Azores-Gibraltar plate boundary is the source of the largest earthquakes and tsunamis in the north Atlantic basin. These include the 1941 M8.4 and 1975 M1979 strike-slip earthquakes west of the Madeira-Tore Rise (MTR) and the 1969, Ms 8.0 earthquake in the Horseshoe Plain south-east of the Gorringe Bank (Buforn et al., 1988; 2004; Fukao, 1973) (Fig. 1). This plate boundary is also believed to have been the source region of the 1722 and 1761 tsunamigenic earthquakes (Baptista et al., 2006) and of the great November 1st, 1755 Lisbon earthquake (Machado, 1966; Moreira, 1985; Johnston, 1996). The earthquake, which was estimated to be of magnitude Mw 8.5-9.0 (e.g., Gutscher et al., 2006), had the largest documented felt area of any shallow earthquake in

Europe (Martinez-Solares et al., 1979; Johnston 1996) and was the largest natural disaster to have affected Europe in the past 500 years. It inflicted up to 100,000 deaths (Chester, 2001) through destruction by ground shaking, ensuing fires and tsunami waves of 5-15 m that devastated the coasts of Southwest Iberia and Northwest Morocco and were even reported as far north as Cornwall, England (Baptista et al., 1998a). Additionally, Grácia et al. (2003a,b) showed clear evidence of submarine landslide deposits from acoustic-backscattering, suggesting that the slope failure process could have contributed to tsunami generation and reports of tsunami waves along the European and Moroccan coasts.

The large tsunami-wave generated by the earthquake also caused damage in the eastern Lesser Antilles, as far north as Newfoundland, Canada and as far south as Brazil (Kozak et al., 2005; Ruffman, 2006). However, no reports were documented from cities along the U.S. East Coast (Reid, 1914; Lockridge et al., 2002; Ruffman, 2006). Table 1 summarizes the tsunami run-up reports from around the Atlantic Ocean (Reid, 1914; Ruffman, 1990, 2006; Baptista et al., 1998a; O'Loughlin and Lander, 2003; Kozak et al., 2005). Fig. 2 shows relevant locations on the map as well as cities along the U.S. East Coast, which existed in 1755.

Although many attempts have been made to characterize the 1755 Lisbon earthquake and tsunami (Johnston 1996; Baptista et al.,1998a,b; Gutscher et al., 2006; Grandin et al., 2007) only one study (Mader, 2001) had considered the far field effects of the tsunami. Studying far field effects is advantageous in determining a possible source location and fault orientation because such effects are less influenced by near-source bathymetry and are unaffected by components of the tsunami wavefield generated by submarine landslides which are significant in the near-field (Gisler et al., 2006), but attenuate rapidly. Mader (2001) generated a numerical model for a source centered at the location of the Mw 7.8, 1969 earthquake (Fig. 1), which provided estimates of the deep water wave amplitudes along the U.S. East Coast and the Caribbean. However, the study did not attempt to characterize the earthquake's source parameters, using instead a 30-m vertical drop of a 300-km radius area as a source; nor did it endeavor to compare tsunami hazard along the U.S. East Coast and the Caribbean from different sources in the region.

In this study we first investigate constraints on the epicenter of the 1755 Lisbon earthquake from far field numerical tsunami simulations. Second, features such as fault

orientation, distance from source, and near-source and regional bathymetry are tested in order to determine what governs tsunami propagation in the Atlantic Ocean. We then assess the tsunami hazard to the U.S. East Coast and the Caribbean from possible future earthquake sources located in the east Atlantic region.

2. Tectonic setting and the 1755 Lisbon earthquake

The eastern end of the Azores-Gibraltar plate boundary, which separates the Eurasian and African plates, is a region of complex bathymetry. Plate kinematic models together with focal mechanisms show that the motion between the two plates is slow (0.7-5 mm/yr) (Argus et al. 1989; Nocquet and Calais, 2004; Fernandes et al, 2007), changing along the boundary from extension in the Azores to compression towards the east that includes the Gorringe Bank and the Gibraltar arc (Fig. 1, inset). The precise location of the plate boundary close to Iberia is uncertain and the plate boundary deformation there might be diffuse over a 200-330 km wide zone (Grimison and Chen, 1986; Hayward et al., 1999). The dominant active structures in this region are the Gorringe Bank Fault (GBF), the Marqués de Pombal Fault (MPF), the St. Vincente Fault (SVF) and the Horseshoe Fault (HSF), which have been studied by several authors (Sartori et al., 1994; Baptista et. al., 2003; Grácia et al., 2003a; Terrinha et al., 2003). These structures and most of the faults in this area trend NE-SW (Borges et al., 2001; Zitellini et al., 2004; Buforn et al., 2004) (Fig. 1).

Thus far the source of the great Lisbon earthquake remains unknown (Gutscher, 2004). A consensus attributed the origin of the earthquake to a structure located between the Gorringe Bank and the Coral Patch Ridge (Machado, 1966; Moreira, 1985; Johnston, 1996) (Fig. 1). Yet the relatively modest surface area of this fault region makes it difficult to explain the high seismic moment of ~$2x10^{22}$ Nm, for a reasonable set of fault parameters (e.g., co-seismic displacement, rigidity, and recurrence) (Gutscher et al., 2006). Three major solutions were proposed based on seismic reflection and multibeam echosounder data, estimates of shaking intensity, and backward ray tracing of tsunami propagation. These fault solutions are shown in Fig. 1 and will be referred later in this paper as:

Gorringe Bank Fault (GBF) – Johnston (1996) and Grandin et al. (2007) suggested a NE-SW trending thrust fault (strike 060°), possibly outcropping at the base of the NW flank of the Gorringe Bank.

Marqués de Pombal Fault (MPF) – Zitellini et al. (2001) and Grácia et al. (2003a) suggested active thrusting along the MPF, located 80 km west of Cape Sao Vincente (strike 020°).

Gulf of Cádiz Fault (GCF) – Gutscher et al. (2002, 2006) and Thiebot and Gutscher (2006) proposed a fault plane in the western Gulf of Cádiz, possibly as part of an African plate subduction beneath Gibraltar (strike 349°).

3. Methodology

3.1 Tsunami model simulations

All simulations presented in this study were generated using COMCOT (Cornell Multi-grid Coupled Tsunami Model) developed by P.L.-F. Liu, X. Wang, S-B. Woo, Y-S. Cho, and S.B. Yoon, at the School of Civil and Environmental Engineering, Cornell University (Liu et al., 1998). All calculations were performed on the Arctic Region Supercomputing Center in Alaska, using the Tsunami Computational Portal at: http://tsunamiportal.nacse.org/wizard.php. COMCOT solves both linear shallow water (LSW) and non-linear shallow water (NLSW) equations in spherical coordinates. Two simplifying assumptions were made to create the initial sea surface deformation, which serve as the initial boundary conditions for the numerical simulations. First, the sea surface responds instantaneously to seafloor earthquake deformation. Second, the initial sea surface displacement is identical to that of the seafloor (Ruff, 2003). The initial sea surface deformation, computed based upon user-provided fault parameters, is identical to the seafloor displacement generated by Coulomb 3.0 (Lin and Stein, 2004; Toda et al., 2005; http://coulombstress.org). Aside from the governing equations, the difference in using linear vs. non-linear hydrodynamic models lies in the boundary conditions. The linear model uses reflective boundary conditions and is therefore unable to perform explicit run-up calculations at the shallow water areas along the coast. On the other hand, the non-linear model uses moving boundary conditions and is capable of explicit run-up calculations. The linear model was used in this study, because no attempt was made to calculate run-up. The output files used for all interpretations are depth and

158 maximum wave amplitude files. The depth file contains the bathymetry of the region
159 where the simulation took place. An ETOPO2, 2551x1457 bathymetry grid with 2
160 arcmin resolution was used for all simulations. The maximum wave amplitude file
161 contains the calculated maximum sea level amplitude for a selected region, throughout
162 an entire simulation run (tsunami propagation time of 10-11.25 hours).
163
164 *3.2 Tsunami theory and numerical model limitations*
165 Tsunami theory has been studied by many authors. The following section sums up
166 tsunami theory based upon Liu et al (1998) and Ward (2002). The leading wave of a
167 tsunami has a wavelength proportional to the longitudinal dimensions of the earthquake
168 source region, which could be several hundreds to a thousand kilometers for a major
169 earthquake. It is considered to be a shallow water gravity wave, where the ocean depth is
170 negligible compared to the wavelength. Its phase speed is proportional to $\sqrt{gh}$, where, g
171 is the acceleration of gravity and h is the water depth in meters. The wave period ranges
172 between several hundreds to several thousand seconds. During propagation in deep water,
173 tsunami wave slope is small, resulting in insignificant convective inertia forces, which
174 can be ignored. As tsunamis propagate into the shallower water region, the wave
175 amplitude increases and the wavelength decreases due to shoaling. The nonlinear
176 convective inertia force becomes increasingly important. In the very shallow water, the
177 bottom frictional effects become significant as well. Therefore, the nonlinear shallow
178 water equations including bottom frictional terms should be used in the description of the
179 tsunami inundation. In principle, numerical computation of wave heights based on linear
180 shallow water equations is sufficient and accurate as long as the modeled tsunami
181 wavelength is much greater than water depth and the wave amplitude is much smaller
182 than water depth. This principle holds up until the deep part of the continental shelf.
183 Consequently, this study is unable to provide definite run-up results and only relative
184 amplitudes can be taken into consideration.
185 The time step chosen for each simulation must meet the Courant-Friedrichs-Lewy
186 (CFL) condition (Courant et al., 1928) in order to assure numerical stability. The CFL
187 condition for explicit numerical methods assures that the algorithm used for solving
188 partial differential equations is convergent. For the COMCOT modified explicit scheme,

189 the largest allowable Courant number is 0.8660 (Liu et al., 1998). Therefore, in order to
190 assure stability the time step used in this study never exceeded 3 seconds.
191
192 *3.3 Tsunami amplitude*
193 Two methods were used to reliably calculate wave amplitude. First, the amplitude
194 was calculated at depths of 250 m (see 'shelf point' in Fig. 3), similar to ten Brink et al.
195 (Chapter 7, 2007), in selected sites along the U.S. East Coast, the Caribbean Islands,
196 Europe, and Africa (Fig. 2). This depth falls within the minimal wavelength to grid size
197 ratio (see section 3.2 for detail), allowing for accurate propagation and amplitude
198 calculations. Second, a rectangular patch of different sizes (Fig. 3) was chosen seaward
199 of each location along the Atlantic, Caribbean, African and European coasts (Fig. 2).
200 The average amplitude was calculated for all of the points within the depth range of 150
201 to 50 m in each patch. The size of the patches varied depending on the geographical
202 locations where the amplitudes are measured. Along the U.S. East Coast for instance,
203 where the shelf is wide, larger patches were selected to account for as many points as
204 possible within the 150 to 50 m depth range. In the Caribbean, where the shelf is
205 narrower, smaller patches were sufficient to incorporate a representative number of
206 points in the same depth range. Although amplitudes calculated at such shallow depths
207 may be inaccurate in terms of their geographical locations, averaging them out over a
208 large area gives a good indication of the wave amplitude in that particular region. This
209 method also verifies that the amplitude calculated at a nearby shelf edge point of 250 m
210 depth is not anomalous. Figs. 4a and 4b show a comparison between amplitudes
211 calculated using the two methods, from an earthquake source located in location 8 (Fig.
212 3). Indeed, the average amplitudes calculated in the patches in the shallower water show
213 similar or higher amplitudes in comparison to the ones calculated in the slightly deeper
214 shelf edge points, as one would expect from the amplification effects of shallow waters.
215
216 *3.4 A method to overcome unreliable historical reports of run-up observations*
217 Caution must be exercised when using historical reports in order to compare between
218 possible epicenter locations. Table 1 shows the variability of run-up amplitudes in
219 historical reports, particularly in the Azores, Madeira, Lisbon and Tangier. It is therefore
220 impossible to compare our model results to individual run-up reports. Moreover, run-up

221 amplitudes are highly sensitive to the near shore bathymetry and onshore topography
222 whereas, because of the model limitations discussed in sections 3.1 and 3.2, amplitudes
223 were calculated at a water depth of 250 m. We therefore grouped together places in the
224 Caribbean, along the Portuguese and Moroccan coast, in Madeira and the Azores, as
225 locations representing consistent reports of high amplitudes. Earthquake sources
226 generating high tsunami amplitudes in those locations are therefore assigned as a good fit
227 to the 1755 Lisbon earthquake epicenter. Similarly, we joined together places along the
228 U.S. East Coast and in Vigo and La Coruña in the northern Spanish coast, under a
229 category of places where no historical reports were documented (i.e., negative evidence).
230 Blank, (2008) quotes a French report from 1756 about a tsunami striking La Coruña, but
231 the report itself does not mention tsunami there (Anonyme, 1756) , we interpret the
232 general lack of reports from this established harbor to indicate that its amplitude was
233 small. The particular locations along the U.S. East Coast (with the exception of Virginia
234 Key in Florida), and Vigo and La Coruña in Spain, were chosen because they were
235 already populated at the time of the earthquake yet there were still no tsunami reports
236 found in the literature. In places along the U.S. East Coast, the tsunami should have
237 struck during daylight hours. The semi-diurnal tidal ranges along the U.S. East Coast are
238 <3 m and the difference between the times that high-tide reaches different locations along
239 the East Coast is as large as 5 hours. Therefore, had a significant tsunami impacted the
240 U.S. East Coast, some sites there would have experienced flooding during low tide. In
241 NW Spain, both the time the tsunami should have struck and the tide conditions are
242 similar to the other locations further south along the coast. Therefore, neither tidal
243 variations nor time of the day are likely to explain the absence of reports in these
244 locations. Table 2 summarizes the criteria used to group the historical reports.
245 In order to quantify the results we compared and normalized the amplitudes of all
246 sources relative to source 5 (shown in Fig. 3). For each location *j* out of a total of *n* along
247 the coasts (shown in Fig. 2 and Table 1) where no amplitudes were reported, we
248 calculated the amplitudes of different model sources relative to that of source 5 using:

249 $$Amp_i^{\min} = \sum_{j=1}^{n} (Amp_5 - Amp_i) / Amp_5 \qquad (1)$$

250 where *i* represents the 16 model epicenter locations shown in Figure 3 . A better
251 fitting epicenter location for any one of the examined model locations along the coasts

would generate wave amplitudes lower than that of source 5 and, thus, receive a positive rating relative to source 5. Similarly, for each location *k* out of a total of *m* where high amplitudes were reported (shown in Fig. 2 and Table 1), we calculated the amplitudes of the sources relative to that of source 5 using

$$Amp_i^{\max} = \sum_{j=1}^{n} (Amp_i - Amp_5) / Amp_5 \qquad (2)$$

where i represents the 16 epicenter locations shown in Figure 3. A better fitting epicenter location for any one of the locations along the coasts would generate wave amplitudes higher than source 5 and, consequently, receive a positive rating relative to source 5. As a result, the best fitting source *i* should maximize:

$$[Amp_i^{\min} + Amp_i^{\max}] \qquad (3)$$

Figures 5, 6, 7 and 17 were created using equations 1,2 and 3. Similar results were also obtained when we excluded the Azores, Madeira and Lisbon, where there was a large variation in the reported run-up amplitude, from the calculations.

4. Results

Fig. 3 and Table 3 show all the earthquake sources that were modeled. To facilitate a meaningful comparison among the models, and for lack of detailed geologic constraints for any of the sources, all the models used the same fault dip, dimensions, slip and rigidity (Table 4) as those proposed for GBF (Johnston, 1996). Gorringe Bank is the most prominent morphological feature in the area and was suggested to be capable of generating an earthquake with a moment magnitude of 1.26×10^{22} Nm, similar to the one calculated for the 1755 Lisbon earthquake (Johnston, 1996). The rigidity value used for the moment magnitude calculation was very high (6.5×10^{10} Pa), to account for a fault that is almost entirely within oceanic mantle lithosphere (Johnston, 1996). Furthermore, the use of a pure thrust fault with rake 90°, would result in the highest possible transoceanic tsunami amplitudes (see Geist, 1999), enabling us to test each individual feature that govern tsunami propagation, separately.

4.1 The effect of fault orientation on tsunami propagation and amplitudes

The first set of simulations was designed to examine the effect of strike orientation on tsunami propagation. Source 3 was chosen for this set because it is the one least susceptible to near-source bathymetric effects in the fault region. The fault strike was

284 rotated 360° at 15° interval. Figure 8 shows the variations of maximum wave amplitude
285 as a function of fault orientation, for sites along the U.S. East Coast and the Caribbean. A
286 pattern of two maxima at fault strikes of 165°-180° and 345° yields the highest
287 amplitudes in the Caribbean. A fault strike of 345° is the equivalent to a thrust fault
288 dipping to the ENE (see dashed fault over source 3 in Figure 3) and was chosen as a
289 reference model. In this configuration, the leading westward propagating wave is a
290 depression phase (ocean withdrawal), followed by an elevation phase (flooding), in
291 agreement with observations from Madeira (Reid, 1914), Brazil (Kozak et al., 2005;
292 Ruffman, 2006), Newfoundland (Ruffman, 1990), and the Caribbean (O'Loughlin and
293 Lander, 2003). The minima are for fault strikes of 75°-90° and 270°-285°. Note that
294 GBF, which was suggested as a possible source for the 1755 Lisbon earthquake
295 (Johnston, 1996) has strike of 60°, close to one of the amplitude minima. Similarly, many
296 of the tectonic features proposed by Zitellini at al. (2004), which are oriented sub-parallel
297 to the Gorringe Bank, would have also generated low tsunami amplitudes for the
298 Caribbean, contrary to observations.
299 Figure 6 compares fault orientations for source 5, one of our two preferred source
300 locations for the 1755 Lisbon earthquake. It shows that according to the criteria
301 developed in Section 3.4, source orientation of 345° fits better than source orientations of
302 330° and 360° and much better than a source oriented at 60°.
303
304 *4.2 The effect of different source locations on tsunami propagation and amplitudes*
305 A fault strike of 345° yields the highest amplitudes in the Caribbean in accordance
306 with historical reports and was therefore used when searching for fault location of the
307 1755 Lisbon earthquake (see section 4.3). Sixteen fault locations were modeled as
308 tsunami sources in the region of study (Fig. 3) and tsunami amplitudes were calculated in
309 locations along the U.S. East Coast and the Caribbean as well as along the European and
310 African coasts. Fault orientation for all locations was assumed to be 345° following the
311 analysis in Section 4.1. Figure 5 shows a comparison between the different source
312 locations relative to source 5. Based on the method outlined in Section 3.4, only source 8
313 fits better than source 5 and source 2 fits slightly worse. Note that source locations 8, 5,
314 and 2 are all located within the Horseshoe Plain. Figure 7 shows a comparison between
315 source 5, source 8 and the three previously suggested source locations GBF, MPF, and

GCF. It is clear that these three source locations are a poorer fit to the observations than sources 5 and 8. Figures 9, 10 and 11 show maximum wave amplitude plots from earthquake sources located in GBF, GCF and MBF respectively. Figures 9 and 10 highlight the same conclusion that is portrayed graphically in Figure 7. The maximum wave amplitude generated from GBF (060°) is seen in a direction that is almost perpendicular to that observed by the historical reports. As a result, the Caribbean Islands are unaffected. Contrary to historical reports the wave amplitudes along the U.S. East Coast, generated from GCF (349°) are high (~0.5m) and spread over a relatively wide area (as far north as Charleston). MPF from Figure 11 cannot be discounted, because it shows that the U.S. East Coast remains relatively untouched and high wave amplitudes are seen in the direction of the Caribbean, thus in agreement with historical reports. Nevertheless, the results shown in Fig. 7 as well as comparing between MPF and sources 5 and 8 (Figs. 13, 14), indicate that MPF is less likely to be the 1755 Lisbon earthquake source.

4.3 The 1755 Lisbon earthquake epicenter and fault strike

Figures 5 and 7 indicate that the most likely epicenter of the 1755 Lisbon earthquake according to our model simulations is in the Horseshoe Plain area of sources 5 and 8 and not in the previously suggested locations: GBF, MPF and GCF. The Horseshoe Plain area is characterized by high seismicity and is cut by NE-SW trending thrust faults which reach the seafloor (e.g., Sartori, 1994, Zitellini, 2004). Figures 6 and 8, however, illustrate that the fault was most likely trending NW-SE as opposed to the previously interpreted NE-SW strike orientation. The only known tectonic feature with a NW-SE trend in this area is the inferred Paleo Iberia-Africa Boundary (PIAB), the equivalent structure to the Newfoundland transform fault on the North American plate, which was formed during the opening of the central Atlantic ocean in the Late-Jurassic-Early Cretaceous (Rovere et al., 2004) (Fig. 1). However, further seismic and multibeam investigations of the west Horseshoe Plain are necessary to test if the PIAB is currently active.

4.4 Near field tsunami travel times

Constraining source location based on tsunami travel time is problematic (Gutscher et al., 2006) due to the inaccuracy of historical reports (e.g., a 30 minute difference in arrival time between Porto Santo and Madeira Islands which are only 50 km apart), due to the possibility of landslide-generated tsunamis, and due to the difficulties in simulating tsunami propagation at shallow depths (see section 3.2)

Nevertheless, we computed travel times to locations of historical reports assuming simple aerial distance, tsunami phase speed of $\sqrt{gh}$ with water depths ranging from 2500 m to 4500 m for sources 5 and 8 and 1000 m to 4000 m from source 2 (Table 5), Travel times from historical reports were listed by Baptista et al. (1998a) and Gutscher et al. (2006). Although source location 2 (near MPF) seems to be the best with respect to some of the historical reports, the overall time differences between source location 2 and sources 5 and 8 is minor, implying that an epicenter located further to the west is not unlikely.

5. Discussion

5.1 The effects of regional and near-source bathymetry on tsunami propagation and amplitude

Regional and near-source bathymetry have a significant effect on tsunami propagation in the Atlantic. In a hypothetical case lacking bathymetric features, a tsunami is expected to propagate uniformly in all directions along great circle paths. Figure 12 shows a plot of maximum wave amplitude across the Atlantic ocean from source 5. The black lines indicate great circles from earthquake source 5 to different locations along the U.S. East Coast and the Caribbean. The trace of relatively high wave amplitudes in the direction of Virginia Key in southern Florida represents the only wave packet closely following a great circle. All other wave amplitude traces relevant to the locations along the U.S. East Coast and the Caribbean suggest that the corresponding wave packets were either dispersed or deflected by various bathymetric features. Figures 13 and 14 show a maximum wave amplitude plot from sources 8 and 5 focusing on far-field and near-source effects, respectively. Figure 14 suggests that the wave propagating eastward toward the Portuguese coast is unaffected by deep ocean bathymetry, whereas Figure 13 implies that propagation westward has a fingering pattern due to wave scattering by bathymetry. The near-source bathymetric elements causing such scattering are the

Gorringe Bank, the Ampere and Coral Patch seamounts as well as Madeira Island and the MTR. These bathymetric elements are much shallower than 1500 m, which is the minimal depth required to scatter a tsunami wave according to the analytical analysis of Mofjeld et al. (2000). The energy is first highly influenced by the Ampere and Coral Patch seamounts as well as the MTR and Madiera Island. Farther to the west, wave propagation seems to be influenced by the Mid-Atlantic ridge; in particular the Azores and the Great Meteor and Cruiser seamounts. Higher amplitudes are shown in the vicinity of these bathymetric elements. However, the wave amplitudes decay quickly behind these bathymetric features because these features tend to attenuate the low frequency waves. On the other hand, tsunami wave energy is inferred to be traversing through the low part of the MTR (arrow in Fig. 14) and later in between the Azores and Great Meteor and Cruiser seamounts, following a great circle toward southern Florida; this wave phase maintains its low frequency content and reaches its trans-Atlantic destination with much higher amplitude. We believe the reason why there are no reports from the 1755 tsunami in southern Florida could be attributed to the northern Bahamas Banks (NBB) which may have acted as a barrier to that area. The rest of the U.S. East Coast remains relatively protected. The northern part of the MTR may have played an important role in shielding the United States, scattering wave energy in that direction. Similarly, the Coral Patch and Ampere seamounts as well as Madeira Island seem to partially scatter the energy in the direction of the Caribbean. The same energy is later scattered a bit more by the Great Meteor and Cruiser seamounts. It is possible that the trace of relatively high amplitudes southward of the Great Meteor seamount may correspond to refracted tsunami energy, responsible for run-up reports in Brazil (Kozak et al., 2005; Ruffman, 2006). Scattering energy by seamounts, however, is relatively ineffective (Mofjeld et al., 2000), allowing enough energy to reach the Caribbean, thus explaining the historical reports. Additional simulations using high-resolution near-shore bathymetry could verify the historical reports claiming that some islands in the Caribbean have experienced greater run-ups than others. Historical run-up reports exist for the entire Antilles arc beginning in Santiago de Cuba and ending in Barbados with the exception of San Juan, Puerto Rico. A possible explanation for the absence of a tsunami report from San Juan is the presence of the ultra-deep Puerto Rico trench (-8350 m) north of San Juan, which may have deflected the energy of the ray path that arrived in a sub-critical angle. (Mofjeld et. al, 2000; Mei,

412 1999). The waves propagating northward (as indicated from the high wave amplitudes),
413 amid the Gorringe Bank and the Josephine seamount and then passing north of the
414 Azores, may have eventually reached Newfoundland, Canada, explaining the historical
415 reports there. Finally, the wave energy that passed southward east of the Coral Patch
416 seamount may explain the historical reports in the Canary Islands (Reid, 1914).
417
418 *5.2 Implications to tsunami hazard to the U.S. East Coast*
419 The effect of near-source bathymetry on tsunami propagation was tested in order to
420 assess tsunami hazard to the U.S. East Coast from possible future earthquakes in the
421 study area. Two sources were compared: one east and one west of the MTR because both
422 regions have the potential to generate sufficiently strong earthquakes (Buforn et al.,
423 1988). For both sources the maximum wave amplitude was calculated for fault strike
424 orientations varying from 0-360° at 15° interval as described in section 4.1. The wave
425 amplitudes were then averaged out over 360° and measured at deep water locations 3500
426 and 4000 km (shown by stars in Fig. 2) from sources 16 and 3, respectively. These deep
427 water locations lie along the azimuths of the U.S. East Coast and the Caribbean coastal
428 sites. A 10% amplitude reduction was factored in to compensate for the difference in
429 distance between 3500 and 4000 km (Ward, 2002) in order to properly compare between
430 the two sources (Fig. 15). If bathymetry had no effect on wave propagation one would
431 expect wave amplitudes to be identical. The fact that amplitudes vary, further
432 demonstrates the significant effect of the bathymetry on transatlantic tsunami
433 propagation. The calculations from source 3 illustrate an amplitude distribution pattern
434 very similar to that depicted in Figures 10 with a maximum in the direction of Virginia
435 Key.). Wave amplitudes from an earthquake source west of the MTR (source 16) show
436 an entirely different amplitude distribution pattern, revealing higher amplitudes in the
437 direction of Baltimore and southward down to Cape Hatteras (Azimuth 292 from source),
438 signifying possible tsunami hazard to these regions. All other places calculated from
439 source 16 show a decrease in amplitudes, except for the waves heading towards
440 Charleston, while the amplitude for Dominica remains relatively unchanged. Figure 16
441 shows a maximum wave amplitude plot from source 16, for a fault with a strike of 30°,
442 west of and adjacent to the MTR. This plot may suggest a possible greater hazard to the
443 U.S. East Coast from earthquakes located in the region west of MTR. We should note,

however, that the region west of MTR has so far generated only strike-slip earthquakes (Grimison and Chen, 1986; Buforn et al., 1988) and relative motion there is predicted by plate kinematic models to be strike-slip (Argus et al., 1989; Nocquet and Calais, 2004). Figure 17 compares all the different earthquake sources relative to source 5 with respect to the U.S. East Coast only (excluding the Virgina Key), in the same way described in section 3.4. In all cases the fault strike was 345°, because it yields the highest amplitudes in the direction of the United States, as shown in Figure 8. Source locations 3 and 1 in the Gulf of Cádiz and locations west and north of the Gorringe Bank are calculated to generate the highest amplitude tsunamis along the U.S. East Coast, highlighting the potential hazard from these sources. Figure 10 further demonstrates the potential tsunami hazard to the U.S. East Coast from earthquake sources located in the Gulf of Cádiz. Figure 11, on the other hand, shows low tsunami risk from an earthquake source located in the MPF. We can therefore conclude that the Gorringe Bank and the north MTR may protect the U.S. East Coast from earthquakes in the Horseshoe Plain, the MPF, the SVF and their surrounding area, but not from the Gulf of Cádiz. Finally, it is important to note that only thrust earthquakes, roughly striking northward may pose tsunami hazard to the U.S. East Coast.

5.3 Other considerations – shelf width

The continental shelf along the U.S. East Coast is much wider than along the Caribbean Islands. The large shelf width may have contributed to the dissipation of tsunami amplitude along the U.S. East Coast and is perhaps one reason for the lack of historical reports from the 1755 Lisbon tsunami. Due to the limitations imposed by the low-resolution bathymetry (section 3.2), we were unable to quantitatively calculate the shelf width effect on wave amplitudes. Nevertheless, Figs. 12 and 13 illustrate that amplitudes in southern Florida are higher than in other areas along the East Coast although the continental shelf in Florida is wider. This suggests that shelf width affects tsunami propagation and amplitudes less than the source fault strike orientation and the seafloor bathymetry along the wave paths.

6. Conclusions

Methodological tsunami simulations based upon historical reports of both far field and near field effects of the November 1st, 1755 Lisbon tsunami suggest three important

conclusions: First, the earthquake seems to have been generated by a NW-SE trending fault located in the center of the Horseshoe Plain, south of the Gorringe Bank. This orientation is almost perpendicular to previously suggested NE-SW trending faults such as GBF and structures south of the Gorringe Bank (Zitellini, 2001). The only known tectonic structure with a NW-SE orientation in this area is the PIAB, although its potential for reactivation remains ambiguous. Moreover, the modeling results allow us to discount the GCF and to a lesser extent the MPF, because both are located too far to the east of the Horseshoe Plain. The GCF can be discounted as a tsunami source because it is predicted to generate relatively high wave amplitudes along the U.S. East Coast, and relatively low ones along the Caribbean. The orientation and location of the MPF are slightly less favorable than our preferred sources in the Horseshoe Plain, even when considering historical reports of tsunami arrival times.

Second, seafloor bathymetry is a significant factor in dictating transatlantic tsunami propagation. In particular, the bathymetry of the Gorringe Bank, the MTR (Josephine Seamount) and the Azores allows waves to reach Newfoundland, but blocks them from reaching most of the U.S. East Coast, with the exception of southern Florida. The Ampere and Coral Patch seamounts, Madeira Island, and the Great Meteor and Cruiser seamounts reduce wave propagation toward the Caribbean. The latter two features partially refract wave energy toward Brazil. Furthermore, high run-up reports in the Caribbean are most likely due to the steep rise in the bathymetry near to shore.

The third conclusion concerns tsunami hazards to the U.S. East Coast from sources located along the eastern Iberian-African plate boundary, which generate sufficiently strong thrust earthquakes. The Gorringe Bank and the north MTR act as near source barriers, protecting most of the U.S. East Coast. For sources located east of MTR and south of the Gorringe Bank, Florida might be at risk if sufficient wave energy manages to pass through the Bahamas. Sources in the Gulf of Cádiz may present a wider hazard to the U.S. East Coast, because they are sufficiently south as to not be affected by the Gorringe Bank, north MTR, and the Azores. For sources located west of the MTR, the risk is shifted northward in the direction of Baltimore.

It is important to note that the interpretations in this report considered relative amplitudes only. High resolution near-shore bathymetry is crucial for more accurate run-up calculations and tsunami hazard assessments.

Acknowledgments

Propagation models were obtained using the Cornell Multi-grid Coupled Tsunami Model (developed by Liu et al., 1998) in the Tsunami Computational Portal; the Portal is a joint project of the Northwest Alliance for Computational Science & Engineering at Oregon State University (www.nacse.org) and the Artic Region Supercomputing Center (www.arsc.edu) at the University of Alaska-Fairbanks. We thank Dylan Keon and Harry Yeh (Oregon State University) and Tom Logan and Elena Suleimani (Arctic Region Supercomputing Center) for assistance with running the models. We would further like to thank Xiaoming Wang (Cornell University) for technical consultations and assistance, Eric Geist (U.S. Geological Survey, Menlo Park) for fruitful discussions, and Hyun-Sook Kim, Jason Chaytor, and Brian Andrews (U.S.Geological Survey, Woods Hole) for technical assistance. Helpful reviews by Eric Geist and Alberto Lopez, two anonymous reviewers, and Editor David Piper are gratfully acknowledged. Roy Barkan thanks the Woods Hole Oceanographic Institution Summer Student Fellowship Program for their financial support and hospitality. Roy Barkan would further like to thank Shmulik Marco (Tel Aviv University) for providing the technical means to complete this study. This study was funded by the U.S. Nuclear Regulatory Commission under NRC Job Number N6408 *Physical study of tsunami sources*.

References

Anonyme, (1756). J. Historique sur les Matie'res du Tems (T. 79) Jan. 1756, 41-45 (http://gallica.bnf.fr/ark:/12148/bpt6k105284f/f2.table).

Argus, D.F., Gordon, R.G., DeMets, C., Stein, S., 1989. Closure of the Africa-Eurasia-North America plate motion circuit and tectonics of the Gloria fault. J. Geophys. Res. 94, 5585-5602.

Baptista, M.A., Heitor, S., Miranda, J.M., Miranda, P.M.A., Mendes Victor, L., 1998a. The 1755 Lisbon earthquake; evaluation of the tsunami parameters. J. Geodyn. 25, 143–157.

Baptista M.A., Miranda, P.M.A., Miranda, J.M., Mendes Victor, L., 1998b. Constraints on the source of the 1755 Lisbon tsunami inferred from numerical modeling of historical data on the source of the 1755 Lisbon tsunami. J. Geodyn. 25, 159–174.

541 Baptista, M.A., Miranda, J.M.., Chierici, F., Zitellini, N., 2003. New study of the 1755
542 earthquake source based on multi-channel seismic survey data and tsunami modeling.
543 Nat. Hazards Earth Sci. Syst. 3, 333–340.
544 Baptista, M.A., Miranda, J.M.., Luis, J.F., 2006. In search of the 31 March 1761
545 earthquake and tsunami sources, Bull. Seismol. Soc. Am., 96, 713-721.
546 Blank, P.L., 2008. The tsunami in Cadiz on 1 Novermber 1755: A critical analysis of
547 reports by Antonio Ulloa and Louis Godin, CRAS2A-2718, 11 pp.
548 Borges,J.F.,Fitas, A. J. S.,Bezzeghoud, M., and Teves-Costa, P., 2001. Seismotectonics
549 of Portugal and its adjacent Atlantic area, Tectonophys., Vol. 337, 373-387.
550 Buforn E., Udías, A., Mézcua, J., 1988. Seismicity and focal mechanisms in south Spain.
551 Bull. Seism. Soc. Am. 78, 2008-2224.
552 Buforn E., M. Bezzegoud, A. Udias, C. Pro, 2004. Seismic Sources on the Iberia-African
553 Plate Boundary and their Tectonic Implications. Pure and Appl. Geophys.,161, 623-
554 626
555 Chester, D.K., 2001. The 1755 Lisbon earthquake. Prog. Phys. Geogr. 25, 363–383.
556 Courant R., Friedrichs, K., Lewy, H., 1928. Über die partiellen Differenzengleichungen
557 der mathematischen Physik. Mathematische Annalen. 100 (1), 32–74.
558 Fernandes R.M.S, Miranda J.M., Meijninger B.M.L., Bos M.S., Noomen R., Bastos L.,
559 Ambrosius B.A.C., Riva R.E.M., 2007. Surface Velocity Field Of The Ibero-
560 Maghrebian Segment Of The Eurasia-Nubia Plate Boundary. Geophys. J.
561 Int. 169 (1), 315-324.
562 Fukao, Y., 1973. Thrust faulting at a lithospheric plate boundary: The Portugal
563 earthquake of 1969. Earth Planet. Sci. Lett., 18, 205-216.
564 Geist, E.L., 1999. Local tsunamis and earthquake source parameters. Adv. Geophysics,
565 39,117-209.
566 Gisler, G., Weaver, R., Gittings, M. L., 2006. SAGE calculations of the tsunami threat
567 from La Palma. Science of Tsunami Hazards, 24, 288-301.
568 Grácia, E., Danõbeitia, J.J., Vergés, J., PARSIFAL team, 2003a. Mapping active faults
569 offshore Portugal (36°N–38°N): Implications for seismic hazard assessment along the
570 southwest Iberian margin. Geology. 31, 83– 86.
571 Grácia, E., Pallas, R., Casas, D., Willmot, V., Grácia -Orellan, J., Danõbeitia, J.J., The
572 Hits Cruise Party, 2003b. Submarine landslides associated to active faulting offshore

573 Portugal (SW Iberian Margin): Paleoseismic implications. EGS–AGU–EUG Joint
574 Assembly, Abstracts from the meeting held in Nice, France, 6–11 April 2003, abstract
575 #13064.
576 Grandin, R., Borges, J.F., Bezzeghoud, M., Caldeira, B., Carrilho, F., 2007. Simulations
577 of strong ground motion in SW Iberia for the 1969 February 28 (Ms=8.0) and the
578 1755 November 1 (M~ 8.5) earthquakes – I. Velocity model. II. Strong ground
579 motion simulations. Geophys. J. Int. 171(2), 807-822(16).
580 Grimison, N.L., and Chen, W., 1986. The Azores-Gibraltar plate boundary: Focal
581 mechanisms, depth of earthquakes and their tectonical implications. J. Geophys. Res.
582 91, 2029-2047.
583 Gutscher, M.A., Malod, J., Rehault, J.P., Contrucci, I., Klingelhoefer, F., Mendes-Victor,
584 L., Spackman, W., 2002. Evidence for active subduction beneath Gibraltar. Geology.
585 30, 1071- 1074.
586 Gutscher, M.-A., 2004. What caused the Great Lisbon earthquake? Science. 305, 1247–
587 1248.
588 Gutscher, M.-A., Baptista, M.A., Miranda, J.M., 2006. The Gibraltar Arc seismogenic
589 zone: Part 2. Constraints on a shallow east dipping fault plane source for the 1755
590 Lisbon earthquake provided by tsunami modeling and seismic intensity.
591 Tectonophysics. 426,153-166.
592 Hayward, N., Watts, A.B., Westbrook, G.K., Collier, J.S., 1999. A seismic reflection and
593 GLORIA study of compressional deformation in the Gorringe Bank region, eastern
594 North Atlantic. Geophys. J. Int. 138, 831-850.
595 Johnston, A., 1996. Seismic moment assessment of earthquakes in stable continental
596 regions –III New Madrid 1811-1812, Charleston 1886 and Lisbon 1755. Geophys. J.
597 Int. 126, 314-344.
598 Kozak, J.T., Moreira, V.S., Oldroyd, D.R., 2005. Iconography of the 1755 Lisbon
599 Earthquake. Academy of Sciences of the Czech Republic, Prague, 82 pp.
600 Lin, J., Stein, R.S., 2004. Stress triggering in thrust and subduction earthquakes, and
601 stress interaction between the southern San Andreas and nearby thrust and strike-slip
602 faults. J. Geophys. Res. 109, B02303, doi:10.1029/2003JB002607.

603 Liu, P.L.-F., Woo, S.-B., and Cho, Y.-S., 1998. Computer Program for Tsunami
604 Propagation and Inundation, sponsored by National Science Foundation.
605 http://ceeserver.cee.cornell.edu/pll-group/comcot_down.htm.
606 Lockridge, P.A., Lowell, S., Whiteside, L.A., Lander, J.F., 2002. Tsunamis and tsunami-
607 like waves of the Eastern United States. Int. J. Tsunami Soc., 20(3), 120-157.
608 Machado, F., 1966. Contribução para o estudo do terremoto de 1 de Novembro de 1755.
609 Rev. Fac. Ciên. De Lisbon. Ser. C, 14, 19-31.
610 Mader, C.L., 2001. Modeling the 1755 Lisbon tsunami. Science of Tsunami Hazards. 19,
611 93-116.
612 Martinez-Solares, J.M., Lopez, A., Mezcua, J., 1979. Isoseismal map of the 1755 Lisbon
613 earthquake obtained from Spanish data. Tectonophysics, 53, 301-313.
614 Mei, C. C., 1989. The Applied Dynamics of Ocean Surface Waves. World Scientific,
615 Section 3, pp. 740, Singapore.
616 Mofjeld, H.O., Titov, V.V., Gonzalez, F.I., Newman, J.C., 2000. Analytic Theory of
617 Tsunami Wave Scattering in the Open Ocean With Application to the North Pacific,
618 NOAA Technical Memorandum OAR PMEL-116.
619 Moreira, V.S., 1985. Seismotectonics of Portugal and its adjacent area in the Atlantic.
620 Tectonophysics. 117, 85-96.
621 Nocquet, J.M., Calais, E., 2004. Geodetic measurements of crustal deformation in the
622 Western Mediterranean and Europe. Pure Appl. Geophys. (161), 661-681.
623 O'Loughlin, K.F., Lander, J.F., 2003. Caribbean tsunamis: A 500-year history from
624 1498-1998, Kluwer Academic Pub., 280 pp.
625 Reid, H.F., 1914. The Lisbon earthquake of November 1, 1755. Bull. Seism. Soc. Am.
626 4(2), 53- 80.
627 Rovere, M., Ranero, C.R., Sartori, R., Torelli, L., Zitellini, N., 2004. Seismic images and
628 magnetic signature of the Late Jurassic to Early Cretaceous Africa-Eurasia plate
629 boundary off SW Iberia. Geophys. J. Int. 158(2), 554–568.
630 Ruff, L.J., (2003). Some aspects of energy balance and tsunami generation by
631 earthquakes and landslides, Pure Apll. Geophys., 160, 2155-2176.
632 Ruffman, A., 1990. Tsunamis of Eastern Canada, 1755- Present (Abstract). Workshop
633 JW.1. Tsunami Sources Around Europe, European Geophysical Society, XV General

634 Assemble, April 23-27, Copenhagen, Denmark. Annales Geophysicæ, Special issue.
635 Abstract JW.1-11, 334-335.
636 Ruffman, A., 2006. From an Ephemerides to 'Observation on The Changes of The Air':
637 Documenting The far-field parameters of the November 1, 1755 "Lisbon" Tsunami in
638 the western Atlantic (Abstract). Atlantic Geoscience Society 32nd Colloquium and
639 Annual Meeting, February 3-4, Greenwhich, Nova Scotia. Program with Abstracts,
640 63-64. Atlantic Geology. 42(1), 111.
641 35. Sartori, R., Torelli, L., Zitellini, N., Peis, D., Lodolo, E., 1994. Eastern segment of
642 the Azores Gibraltar line (central-eastern Atlantic): An oceanic plate boundary with
643 diffuse compressional deformation. Geology. 22, 555–558.
644 Ten Brink, U., Twichell, D., Geist, E., Chaytor, J., Locat, J., Lee, H., Buczkowski, B.,
645 and Sansoucy, M., 2007. The current state of knowledge regarding potential tsunami
646 sources affecting U.S. Atlantic and Gulf Coasts, U.S. Geological Survey
647 Administrative Report, pp. 162.
648 Terrinha, P., Pinheiro, L.M., Henriet, J.-P., Matias, L., Ivanov, M.K., Monteiro, J.H.,
649 Akhmetzhanov, A., Volkonskaya A., Cunha, T., Shaskin, P., Rovere, M., 2003.
650 Tsunamigenic-seismogenic structures, neotectonics, sedimentary processes and slope
651 instability on the southwest Portuguese Margin. Mar. Geol. 195, 55-73.
652 Thiebot, E., Gutscher, M.A., 2006. The Gibraltar Arc seismogenic zone (part 1):
653 Constraints on a shallow east dipping fault plane source of the 1755 Lisbon
654 earthquake provided by seismic data, gravity and thermal modeling. Tectonophys.,
655 v.426(in press). 1-2, p.135-152. Tectonophysics, v.426(in press). 1-2, p.135-152.
656 Toda, S., Stein, R.S., Richards-Dinger, K., Bozkurt, S., 2005. Forecasting the
657 evolution of seismicity in southern California: Animations built on earthquake stress
658 transfer. J. Geophys. Res. B05S16, doi:10.1029/2004JB003415.
659 Ward, S.N., 2002. Tsunamis. Encyclopedia of Physical Science and Technology-
660 Academic Press. 17, 175-191. http://es.ucsc.edu/~ward/papers/tsunami_ency.pdf
661 Zitellini, N., Mendes-Victor, L., Córdoba, D., Dañobeitia, J., Nicolich, R., Pellis, G.,
662 Ribeiro, A,Sartori, R., Torelli, L., Bartolomé, R., Bortoluzzi, G., Calafato, A.,
663 Carrilho, F., Casoni, L., Chierici, F., Corela, C., Correggiari, A., Della Vedova, B.,
664 Gràcia, E, Jornet, P., Landuzzi, M., Ligi, M., Magagnoli, A., Marozzi, G., Matias,
665 L.M., Penitenti, D., Rodriguez, P., Rovere, M., Terrinha, P., Vigliotti, L., Zahinos

Ruiz, A., 2001. Source of the 1755 Lisbon earthquake and tsunami investigated. EOS Trans. Amer. Geophys. U. 82, 285.

Zitellini, N., Rovere, M., Terrinha, P., Chierici, F., Matias, L., BIGSETS team, 2004. Neogene through Quaternary tectonic reactivation of SW Iberian passive margin. Pure Appl. Geophys. 161, 565– 587.

Figure Captions

Fig. 1. Plate tectonic setting (inset) and bathymetric map of the Iberian-African plate boundary. Depth contours: Blue – 250 m; black – 1000, 1500, and 2000 m.
Barbed lines - proposed faults by previous studies: GBF - Gorringe Bank Fault; MPF - Marqués de Pombal Fault; SVF- St. Vincente Fault; HSF - Horseshoe Fault; GCF - Gulf of Cádiz Fault. PIAB refers to the Paleo Iberia- Africa Plate Boundary (Rovere et al., 2004). Plates in inset: NAM – North America; EUR- Eurasia; AFR- Africa (after Grácia et al., 2003a).

Fig. 2. Locations of run-up reports in Table 1 (red circles) except for Itamaraca and Tamandare (located in Brazil). Also shown are locations along the U.S. East Coast and Spain with no historical reports (open red circles).
Rectangles represent patches used to calculate average tsunami amplitudes on the shelf (see section 3.3 for explanation).
Stars indicate points where average amplitudes over 360 degrees were measured (see section 5.2 for explanation).

Fig. 3. Bathymetric map of the Iberian margin. Contours- same as Fig. 1. Epicenter (placed in the center of finite fault) used to generate tsunami simulations are shown in green circles with corresponding fault model number (see Table 3 for.source coordinates). Fault orientation for sources 3 and 16 were rotated 360° at 15° interval to test for the optimal strike angle generating maximum amplitudes in the Caribbean (see section 4.1 for explanation) to assess the tsunami hazard to the U.S. East coast (see section 5.2 for explanation). Blue circles along the 250 m contour line represent the *shelf points* where the tsunami amplitude was calculated seaward of each historical location.

699 Rectangles- same as in Fig. 2. Red circles represent cities with historical tsunami reports
700 (see Table 1).
701
702 Fig. 4. Comparison between absolute tsunami amplitudes for fault source location 8
703 measured at the shelf edge points at 250 m depth and averaged over rectangular patches
704 at depths of 50-150 m (see section 3.3 for explanation) for the Caribbean side (a) and for
705 the European and African side (b).
706
707 Fig. 5. Comparison between all fault sources shown in Fig. 3 and listed in Table 3. All of
708 the faults have strike of 345° and their other parameters are listed in Table 4. Positive
709 bars represent sources that are better fitting than source 5 to be the 1755 Lisbon epicenter.
710 Negative bars represent sources that are worse fitting than source 5 to be the 1755 Lisbon
711 epicenter (see section 3.4 for explanation). According to this test source 8 is the best
712 candidate source for the 1755 Lisbon earthquake.
713
714 Fig. 6. Comparison between tsunami amplitude from different fault orientations located
715 in source 5. Negative bars represent fault orientations that do not fit as well as the model
716 with strike of 345° (see section 3.4 for explanation). A strike of 60°, like the one
717 suggested for GBF, has the worst fitting.
718
719 Fig. 7. Comparison between sources 5 an 8 and the previously suggested sources of the
720 1755 Lisbon earthquake: GBF (Johnston, 1996); MPF (Zitellini et al., 2001); and GCF
721 (Gutscher et. al, 2006) (sources 7, 4 and1 respectively); fault strikes were 060°, 020° and
722 349°, respectively. Positive bars represent source locations that are better fitting than
723 source 5 to be the 1755 Lisbon epicenter. Negative bars represent source locations that
724 are less fitting than source 5 to be the 1755 Lisbon epicenter (see section 3.4 for
725 explanation). Both Sources 5 and 8 are better fitting than the three previously suggested
726 fault models.
727
728 Fig. 8. Comparison between the absolute tsunami amplitudes as a function of variation in
729 the fault strike orientation, using source 3. Maxima are at 165°-185° and 345° and
730 minima are at 75°-90° and 270°-285°.

Fig. 9. Maximum wave amplitude from an earthquake source located in GBF. The strike angle used is 60° similar to that suggested by Johnston (1996) and Grandin et al. (2007). The scale ranges from 0-2 m, with 0.1 m intervals. The main wave energy propagates NNW, leaving the Caribbean Islands almost unaffected.

Fig. 10. Maximum wave amplitude from an earthquake source located in GCF with fault strike of 349° similar to that suggested by Gutscher et al. (2002; 2006) and Thiebot and Gutscher (2006). Scale- same as in Fig. 9. Contrary to historical records low amplitudes are seen in the vicinity of the Caribbean, whereas high amplitudes are seen along the U.S. East Coast, south of Charleston.

Fig. 11. Maximum wave amplitude from an earthquake source located in MPF with fault strike of 20°. Location and strike are after Zitellini et al. (2001) and Grácia et al. (2003a). Scale- same as in Fig. 9. Note that although a tsunami generated at the MPF is not expected to affect the U.S. Atlantic coast, it predicts lower amplitude in the Caribbean and higher amplitude in northwest Spain than Fig. 13.

Fig. 12. Maximum wave amplitude projected on a sphere from an earthquake source located in source 5. The scale ranges from 0-1 m. Warm colors indicate high amplitudes and cold colors low amplitudes. Black lines indicate great circle paths between source 5 and locations along the U.S. East Coast and the Caribbean. The wave energy heading toward Virginia Key in southern Florida is the only one following a great circle path. All other wave energies are scattered by topography.

Fig. 13. Maximum wave amplitude from the best fit earthquake source located in source 8. Scale- same as in Fig. 9. Wave scattering is mainly caused by the Madeira Island, Madeira Tore-Rise (MTR), the Azores, the Great Meteor (GM) and Cruiser (Cr) seamounts. The ray passing in between the Azores and the Great Meteor seamount reaches southern Florida. The rest of the U.S. East Coast is relatively unaffected by the tsunami. NBB-northern Bahamas Banks.

763 Fig. 14. Maximum wave amplitude from an earthquake source located in source 5,
764 illustrating the effects of near-source topography. The scale ranges from 0-5 m, with 0.1
765 m intervals. Tsunami propagation eastward is undisturbed by topography. High
766 amplitudes in the Gorringe Bank, Coral Patch (CP) and Ampere (Amp) seamounts, and
767 Madeira Tore-Rise (MTR) are due to wave amplification by these relatively shallow
768 features (> -1500 m), although these features scatter the long period component (see
769 section 5.1 for explanation). The arrows represent a less-attenuated wave, which traverses
770 between the Azores and the Great Meteor seamount heading toward southern Florida (see
771 Fig. 13). Jos. Smt.- Josephine seamount.
772
773 Fig. 15. Comparison of tsunami amplitudes from sources located to the east (source 3)
774 and the west (source 16) of the MTR. Amplitudes are measured in deep water 4000 km
775 west from source 3 and 3500 km west from source 16 (see stars in Fig. 2). The
776 amplitudes are measured in the direction of sites along the U.S. East Coast and the
777 Caribbean as indicated at the bottom of each bar. Amplitudes from source 16 were
778 reduced by 10% in order to compensate for the 500 km shorter propagation path relative
779 to source 3 (Ward, 2002). Amplitudes were averaged over 24 fault orientations covering
780 360° at 15° interval. Differences in amplitudes illustrate the effect of the bathymetry on
781 tsunami propagation, in particular the effects of the north MTR.
782
783 Fig. 16. Maximum wave amplitude from an earthquake source located in source 16 and
784 oriented 30°. Scale- same as Fig. 9. High amplitudes are seen in a wider area along the
785 U.S. East Coast relative to Fig. 13, highlighting the greater hazard from earthquake
786 sources located west of MTR.
787
788 Fig. 17. Comparison between all of the modeled sources relative to source 5, for sites
789 along the U.S. East Coast (see section 3.4 for explanation). See Figure 3 and Table 3 for
790 source locations. Positive bars represent sources that may have a lower impact than
791 source 5 on the U.S. East Coast. Negative bars represent sources that are calculated to
792 have greater impact than source 5 to the U.S. East Coast (see section 5.2). Sources 1, 3,
793 12, 16 and 10 are calculated to have the greatest impacts to the U.S. East Coast.
794

Table 1
Click here to download Table: Table 1.doc

Table 1- Sites of historical tsunami runup reports, sites that were populated in 1755 but did not mention tsunami impact and sites with tsunami reports but no run-up reports

Location	Latitude (°N)	Longitude (°E)	Run-up (m)	Reference
Santiago de Cuba	20.010	-75.810	NRR	OL
Samaná Bay	19.139	-69.355	NRR	OL
St. Martin	18.060	-63.050	4.5	OL
Saba	17.630	-63.230	?-7	OL, Ba2, Ru
Antigua	17.090	-61.800	3.6	OL
Dominica	15.300	-61.380	3.6	OL
Barbados	13.250	-59.530	1.5-1.8	OL,Ba2
Itamaraca (Brazil)	-7.747	-34.825	NRR	Ru
Tamandare (Brazil)	-8.760	35.105	NRR	Ru
Bonavista	49.000	-53.333	NRR	Ru ,Re
Boston	42.358	-71.060	NR	
Baltimore	39.286	-76.615	NR	
New York	40.716	-74.000	NR	
Charleston	32.783	-79.933	NR	
Virginia Key	25.787	-80.216	NR	
Cornwall	50.130	-5.425	2-3.7	Ba2
La Coruña	43.366	-8.383	NR	
Vigo	42.237	-8.721	NR	
Porto	41.150	-8.633	1	Ba
Figueira	40.140	-8.880	NRR	Ba
Porto Novo	39.100	-9.430	NRR	Ba
Lisbon	**38.700**	**-9.183**	**5-15.2**	**Ba2, OL**
Oeiras	38.683	-9.316	>6	Ba
Angra (Azores)	**38.650**	**-27.216**	**?-14.6**	**Ba2**
Huelva	37.250	-6.950	NRR	Ba
S. Vicente	37.000	-8.990	>10	Ba
Cádiz	36.533	-6.300	15-18.3	Ba, OL
Gibraltar	36.143	-5.353	2	Ba
Ceuta	35.888	-5.312	2	Ba
Tangier	**35.766**	**-5.800**	**?-15.2**	**Ba, OL**
Porto Santo	33.066	-16.330	3	Ba
Madeira	**32.630**	**-16.880**	**4-13.2**	**Ba, OL**
Safi	32.283	-9.233	>6	Ba
Canary Islands	28.135	-15.435	NRR	Re

Run-up reports from Baptista et al., 1998a (Ba1); Baptista et al., 2003 (Ba2); O'Loughlin and F. Lander, 2003 (OL); Ruffman, 1990, 2006 (Ru); Reid, 1914(Re)
Madeira, Lisbon, Angra and Tangier are bolded to indicate the large uncertainty regarding historical run-up amplitudes in those regions
NRR- Tsunami report but no run-up report
NR- No tsunami report

Table 2
Click here to download Table: Table 2new.doc

Table 2- Regions of reported tsunami run-ups (High) and regions were no run-ups were reported (Low)

	Far field	**Near field**
High run-up region	Caribbean	Lisbon to Morocco, Azores, Madeira
Low run-up region	U.S. East Coast	NW Spain

Table 3
Click here to download Table: Table 3new.doc

Table 3- Geographical coordinates of source locatioas shown in figure 3

Source Number	Latitude (°N)	Longitude (°E)
1	35.480	-8.200
2	36.210	-9.825
3	***35.144***	***-10.055***
4	37.150	-10.110
5	36.042	-10.753
6	37.045	-10.780
7	36.940	-11.450
8	36.015	-11.467
9	37.957	-12.052
10	36.835	-12.120
11	36.789	-13.039
12	36.300	-13.051
13	37.991	-13.414
14	37.205	-13.606
15	37.507	-14.514
16	***36.748***	***-15.929***

Source locations are measured in the center of each finite fault
Bolded sources were rotated 360° and used to generate figure 15

Table 4
Click here to download Table: Table 4new.doc

Table 4- Fault parameters used for all simulations

Source Depth (Km)	Fault Length (Km)	Fault Width (Km)	Average Slip (m)	Dip (deg)	Rake (deg)
5	200	80	13.1	40	90

Source depth corresponds to the top of the fault plane

Table 5

Click here to download Table: Table 5new.doc

Table 5- Comparison of historically observed tsunami arrival times with calculated arrival times from sources 5, 8 and 2 (S5, S8 and S2) in Figure 3 and compared to calculated arrival times from two sources (1 and 2) at the Marques de Pombal "source B"(N 160) and "source C" (N160N135) (Baptista et al., 1998b) and a source in the Gulf of Cadiz (Gutscher et al., 2006)

Location	Historical time	Travel time S5	Travel time S8	Depth (m)	Travel time S2	Depth (m)	Travel time MPF1	Travel time MPF2	Travel time GCF
St. Vincente	16 ± 7	16-17	21-22	*4000-3500*	16-19	*1500-1000*	25	21	22
Huelva	50 ± 10	39-44	45-51	*2500-2000*	39-47	*1500-1000*	80	74	52
Cadiz	78 ± 15	43-48	50-56	*2500-2000*	44-54	*1500-1000*	70	70	36
Gibraltar		52-58	59-66	*2500-2000*	55-68	*1500-1000*			53
Tangiers		48-53	54-61	*2500-2000*	50-62	*1500-1000*			54
Porto Santo	60 ± 15	48-51	44-47	*4500-4000*	58-62	*4000-3500*	68	70	59
Madeira	90 ± 15	54-57	49-52	*4500-4000*	64-68	*4000-3500*	78	78	72
Safi	26-34	35-37	37-39	*4500-4000*	37-40	*4000-3500*	75	81	55
Orieas	25 ± 10	34-38	37-42	*2500-2000*	38-47	*2000-1500*	28	22.6	51
Lisbon		35-39	38-43	*2500-2000*	39-48	*1500-1000*			
Figueira	45 ± 10	52-58	54-61	*2500-2000*	61-75	*1500-1000*	53	50	83
Porto		63-71	66-74	*2500-2000*	76-94	*1500-1000*	90	87.5	96

All times are in minutes.

Figure 1

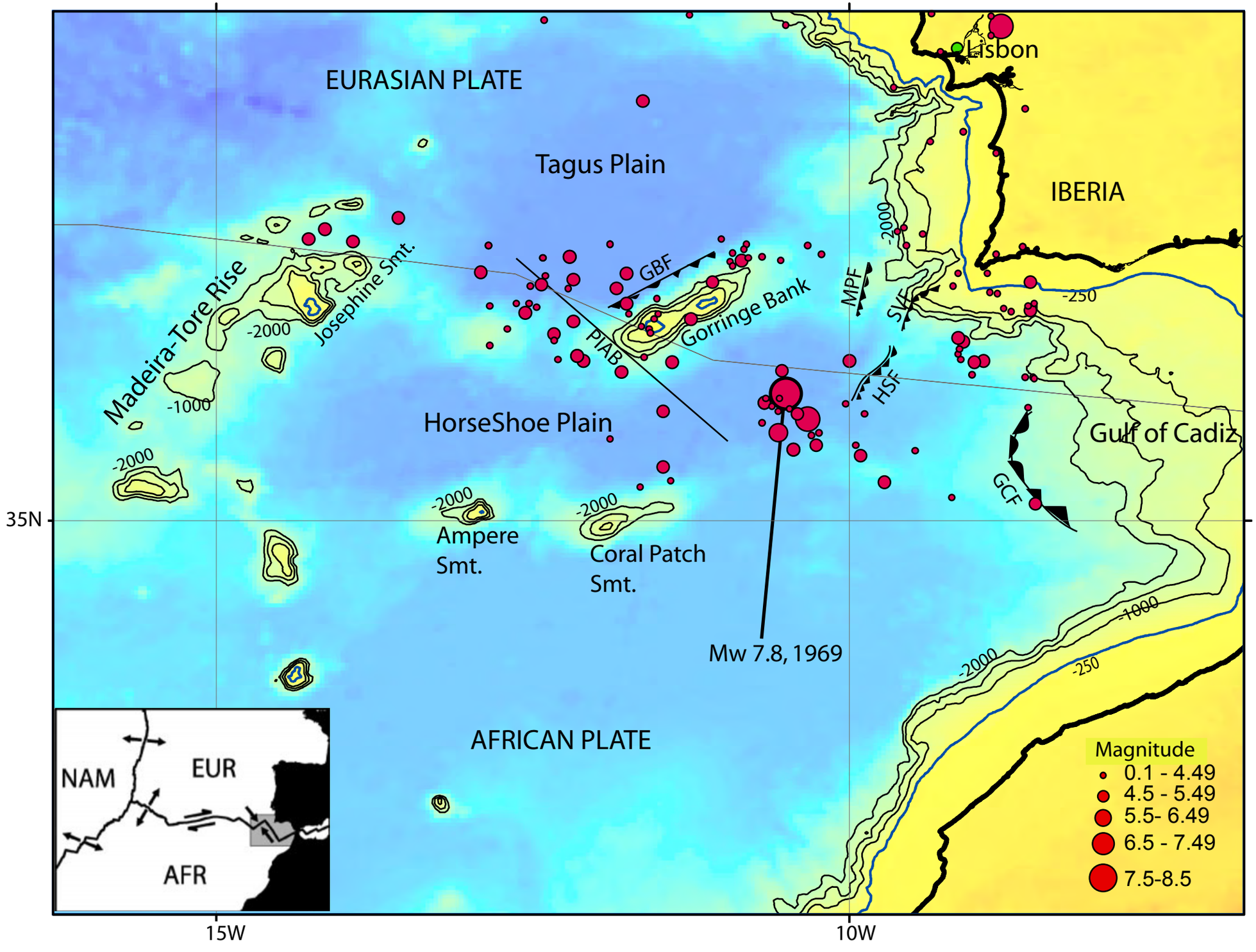
EURASIAN PLATE
Tagus Plain
Lisbon
IBERIA
Madeira-Tore Rise
Josephine Smt.
-2000
-1000
GBF
PIAB
Gorringe Bank
MPF
SVF
-2000
-250
HSF
HorseShoe Plain
Gulf of Cadiz
GCF
-2000
-2000
-2000
Ampere
Smt.
Coral Patch
Smt.
Mw 7.8, 1969
35N
-1000
-2000
-250
AFRICAN PLATE
NAM
EUR
AFR
Magnitude
0.1 - 4.49
4.5 - 5.49
5.5- 6.49
6.5 - 7.49
7.5-8.5
15W
10W

Figure 2

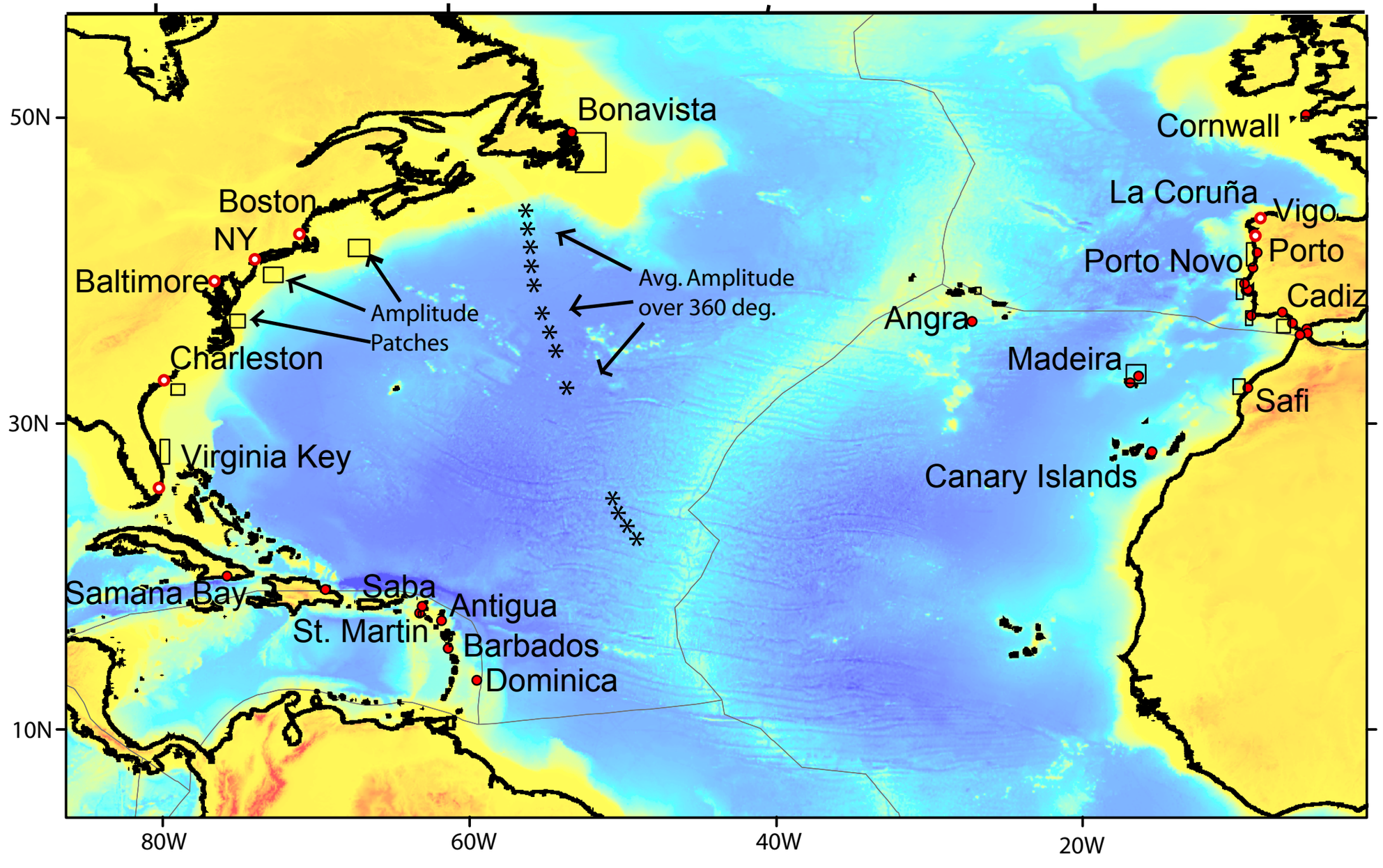

Figure 2.

Figure 3

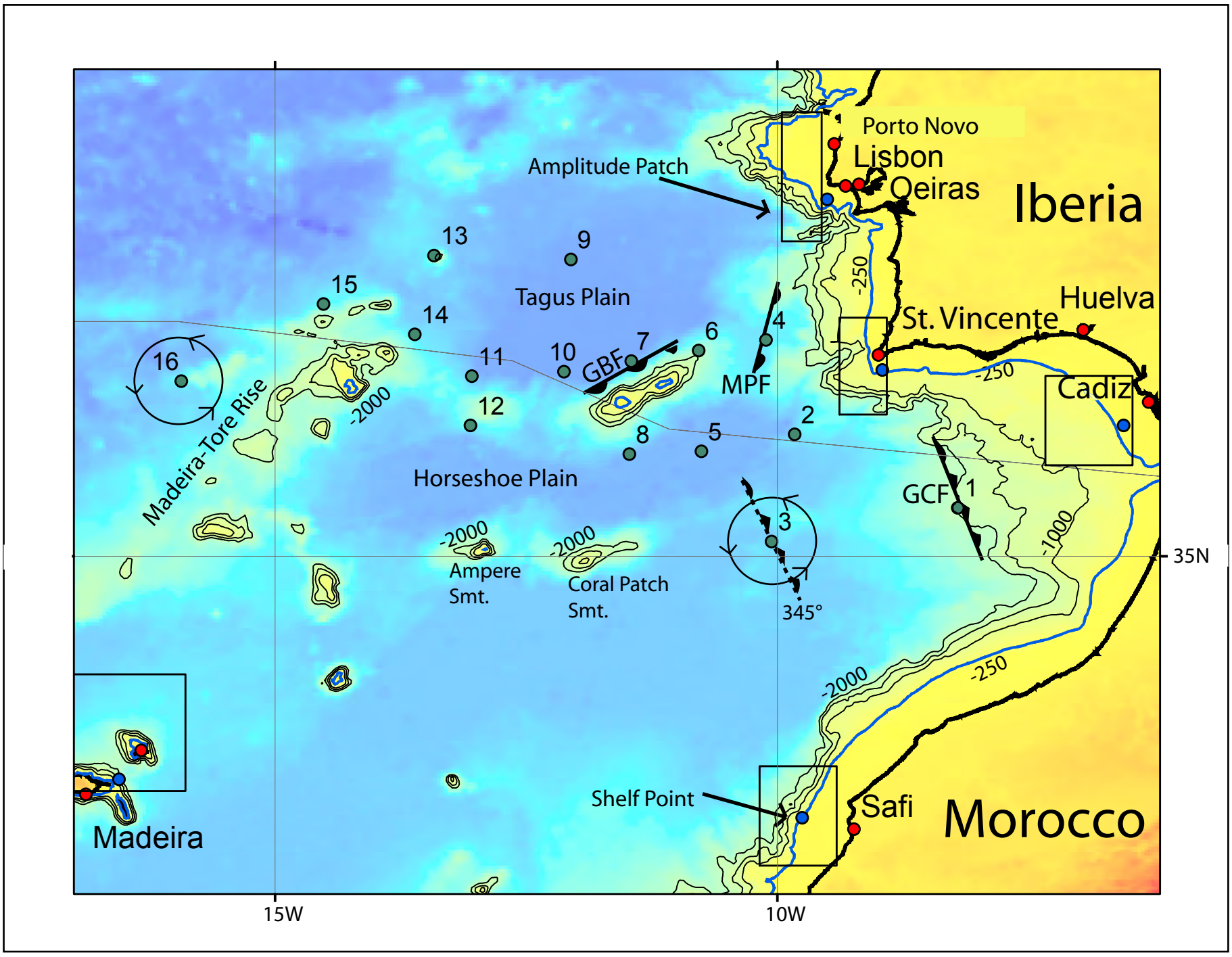

Figure 3

Figure 4

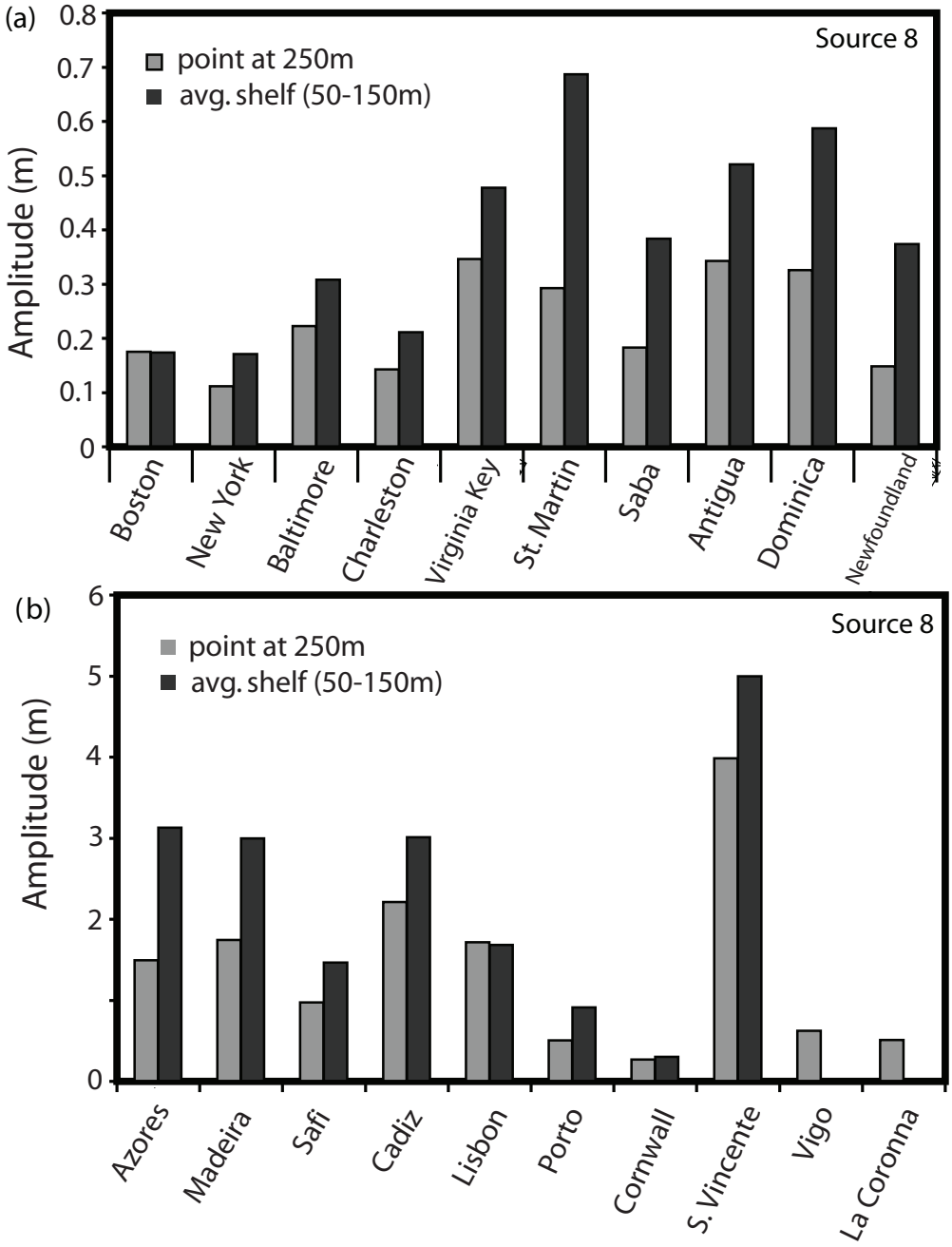
(a)
Source 8
point at 250m
avg. shelf (50-150m)
Amplitude (m)
0
0.1
0.2
0.3
0.4
0.5
0.6
0.7
0.8
Boston
New York
Baltimore
Charleston
Virginia Key
St. Martin
Saba
Antigua
Dominica
Newfoundland
(b)
Source 8
point at 250m
avg. shelf (50-150m)
Amplitude (m)
0
2
3
4
5
6
Azores
Madeira
Safi
Cadiz
Lisbon
Porto
Cornwall
S. Vincente
Vigo
La Coronna

Figure 5

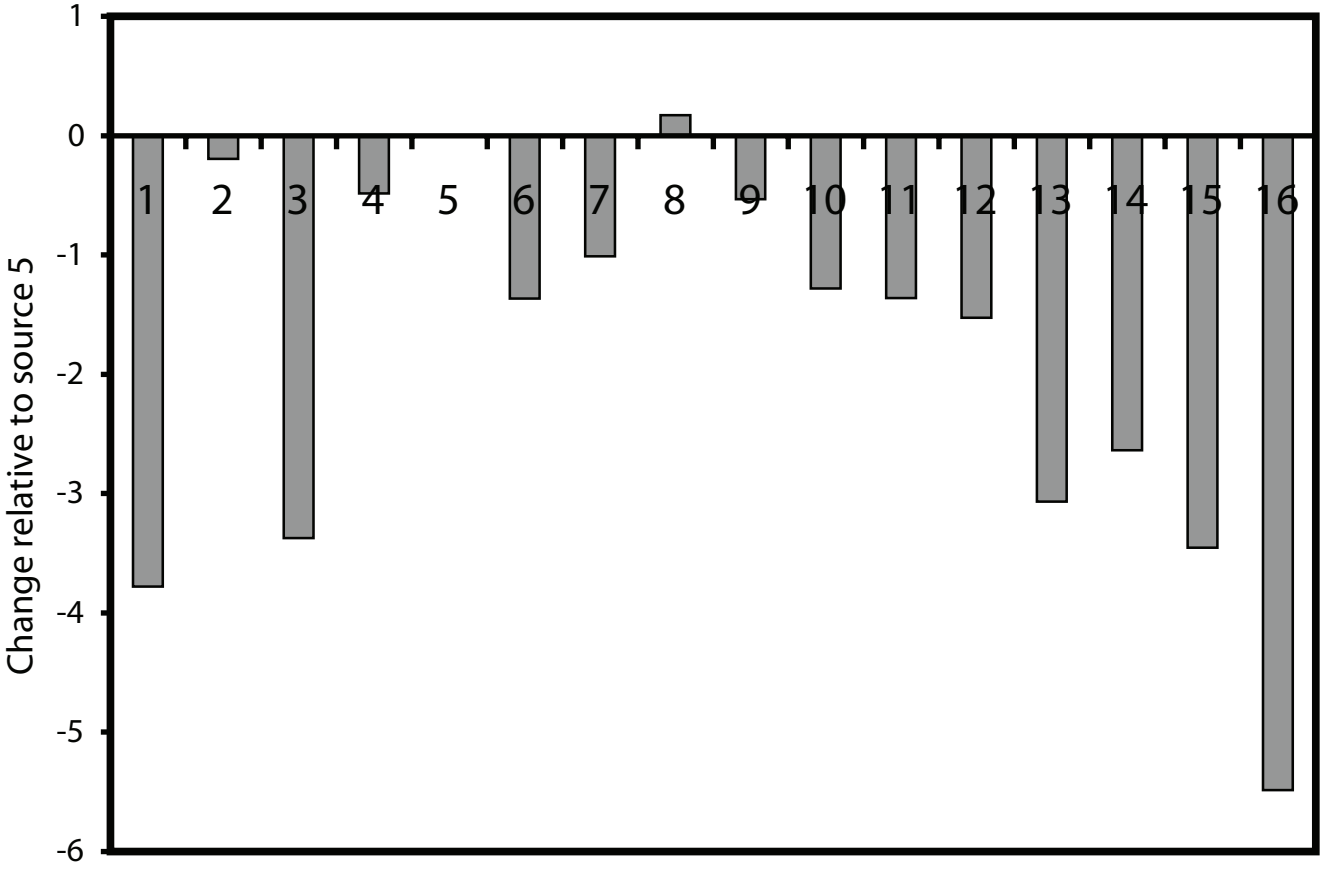
1
0
-1
-2
-3
-4
-5
-6
Change relative to source 5
1
2
3
4
5
6
7
8
9
10
11
12
13
14
15
16

Figure 6,7

Fig. 6

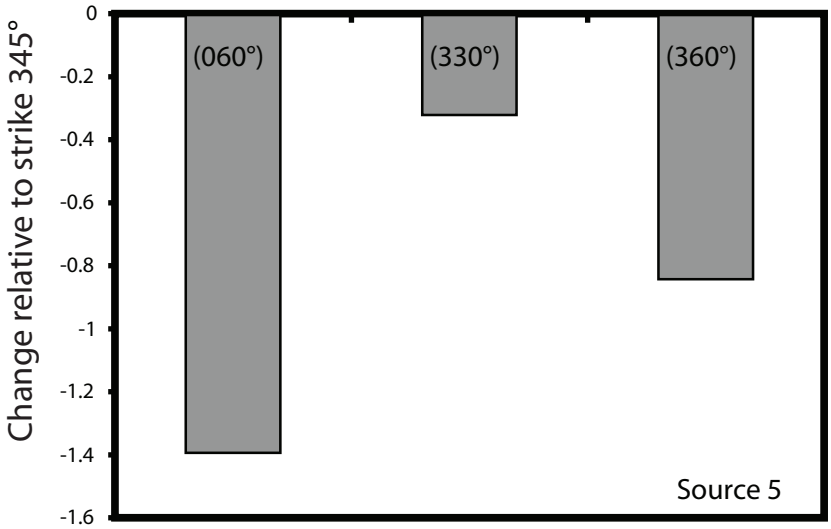

Fig. 7

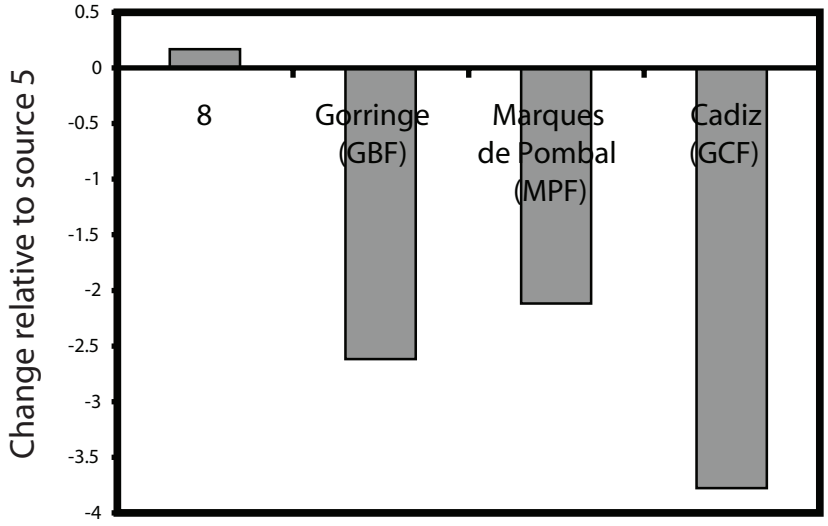

Figure 8

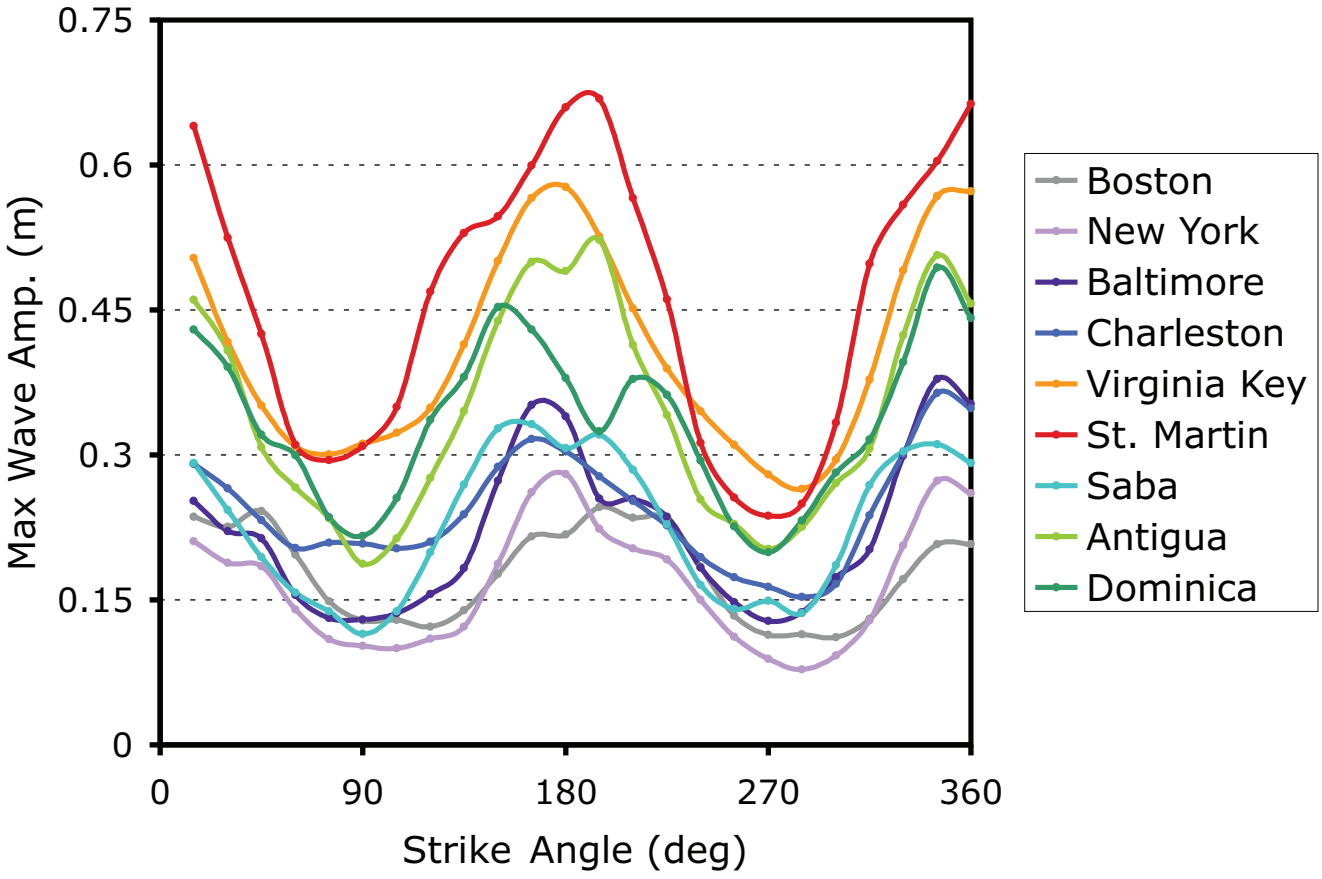
0.75
0.6
0.45
0.3
0.15
0
Max Wave Amp. (m)
0
90
180
270
360
Strike Angle (deg)
Boston
New York
Baltimore
Charleston
Virginia Key
St. Martin
Saba
Antigua
Dominica

Figure 9

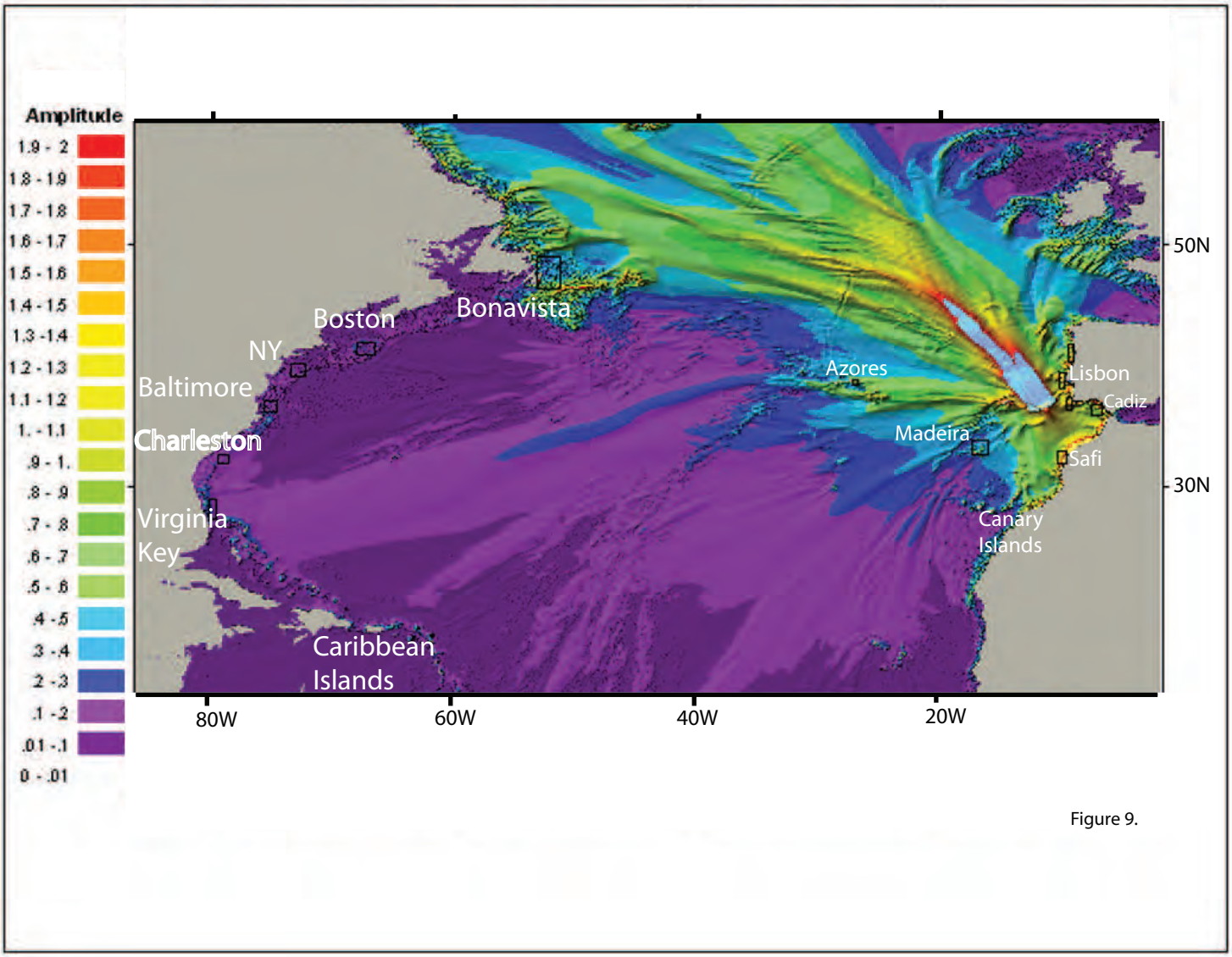

Figure 9.

Figure 10

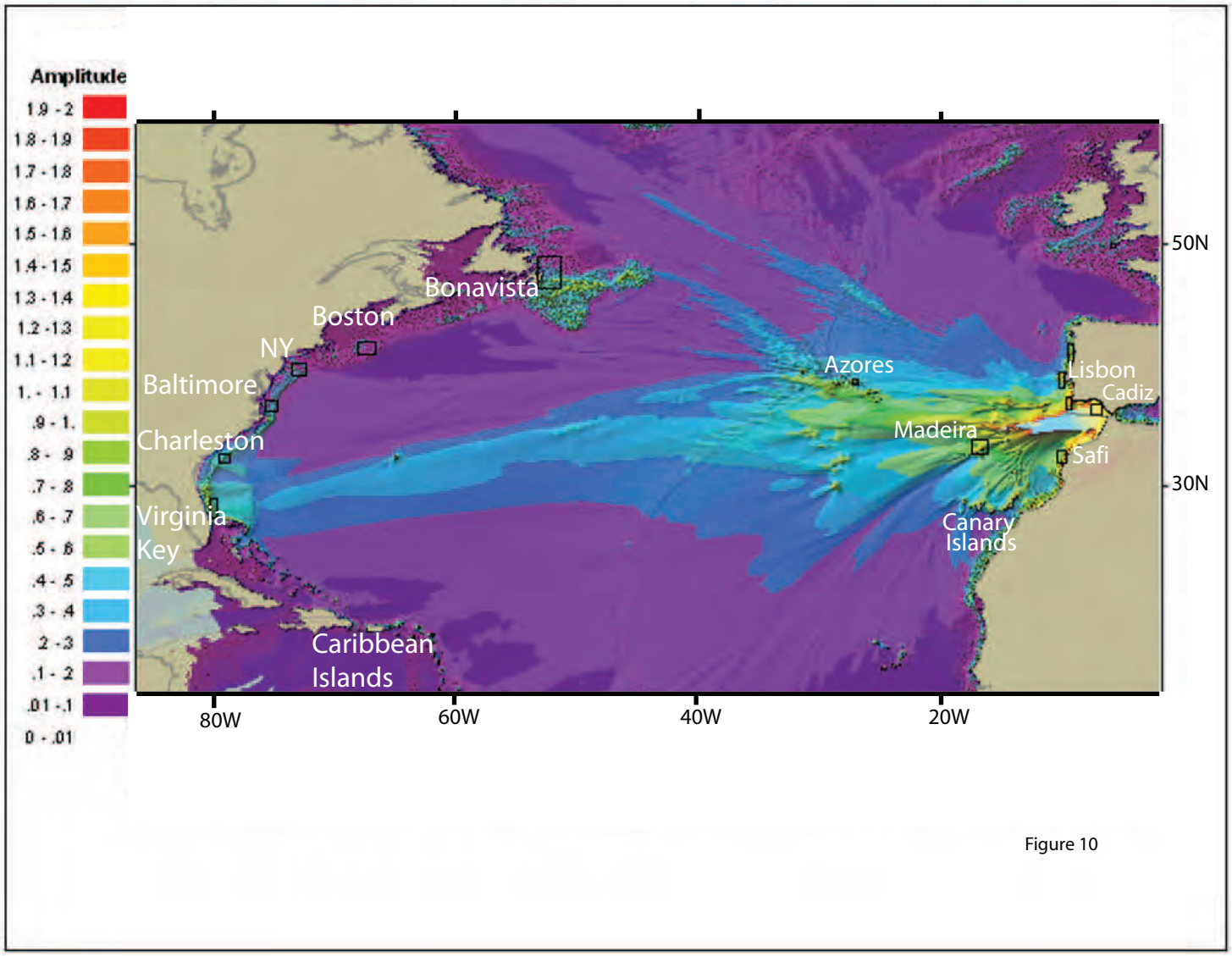

Figure 10

Figure 11

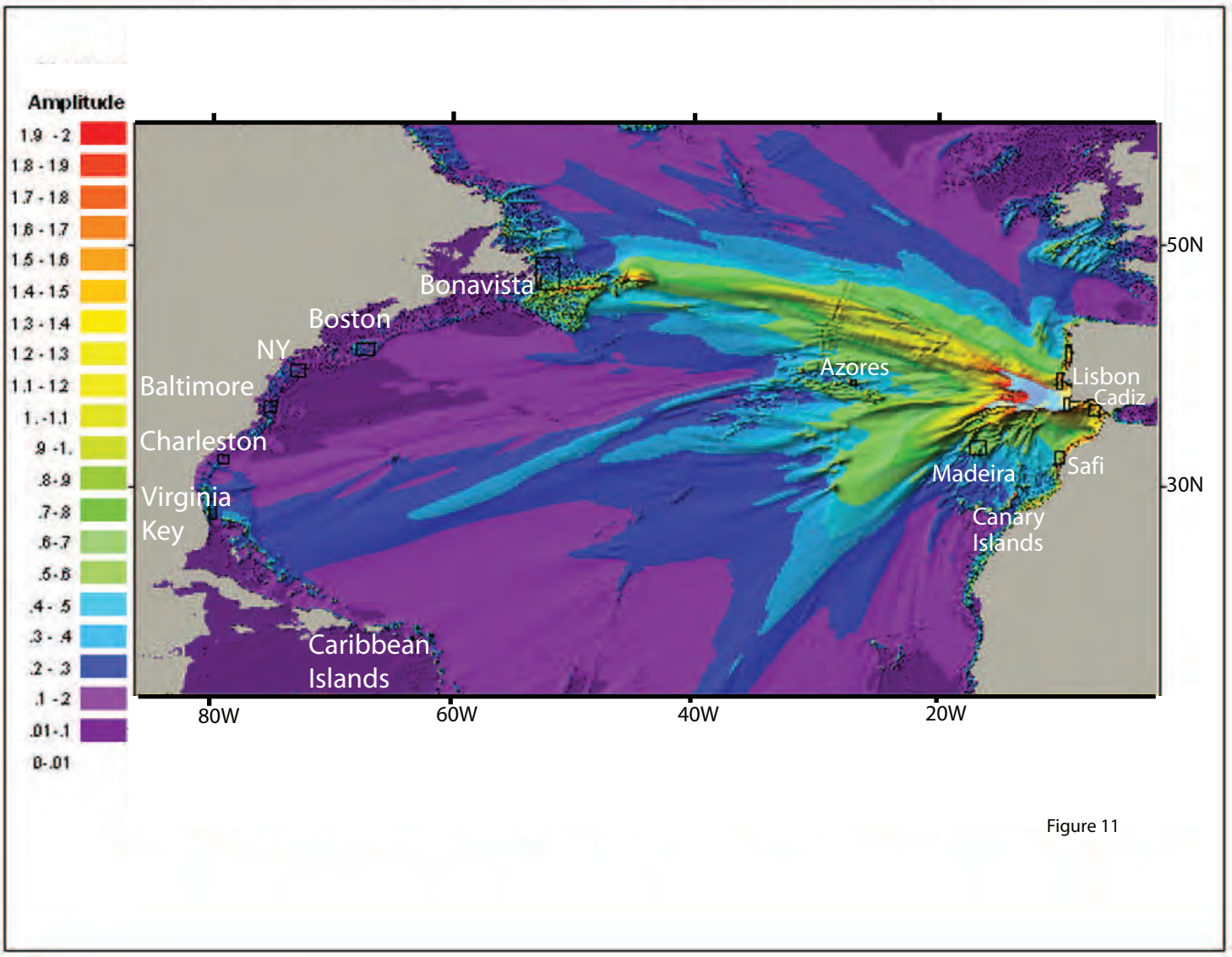

Figure 11

Figure 12

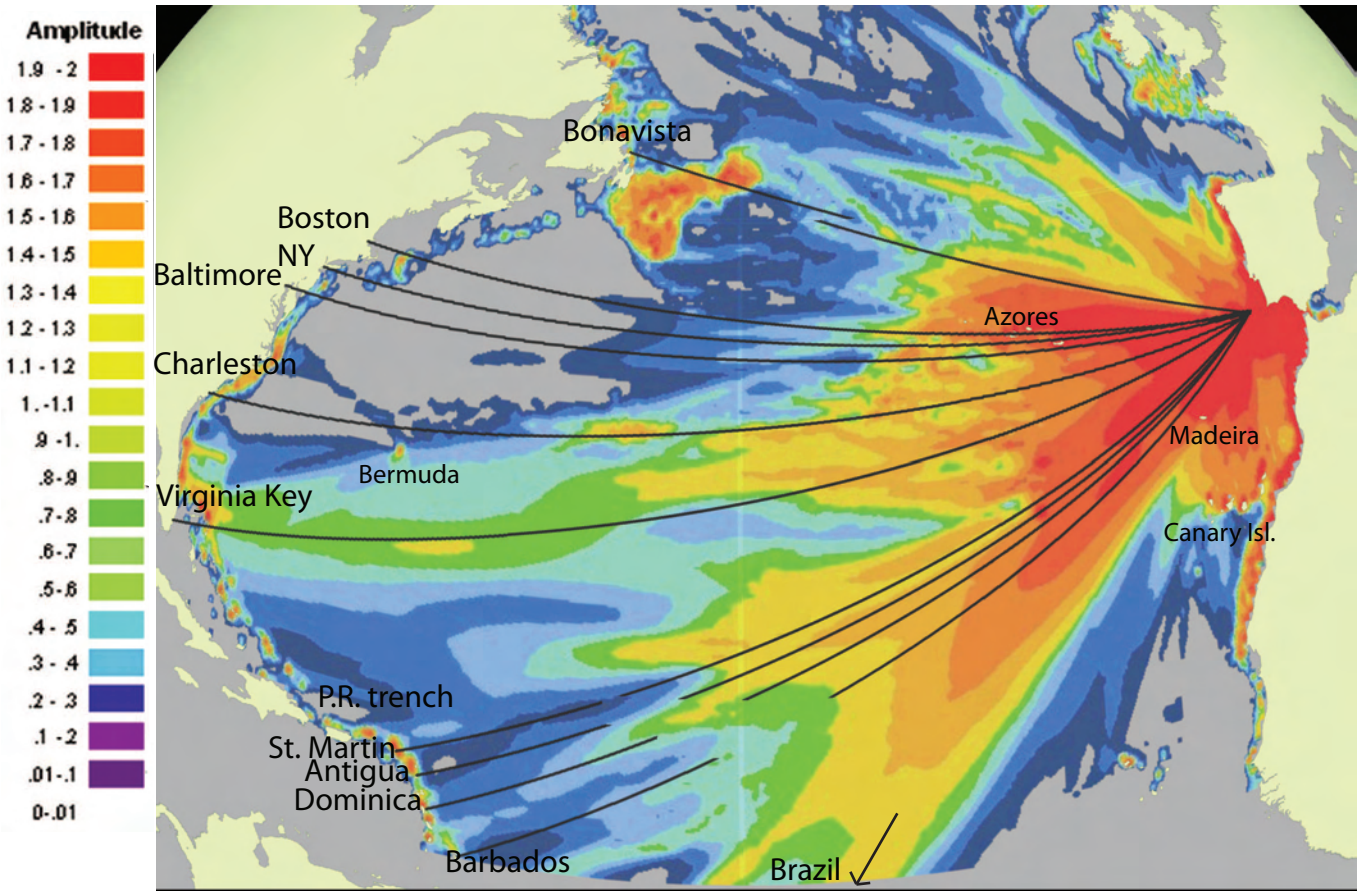

Figure 12.

Figure 13

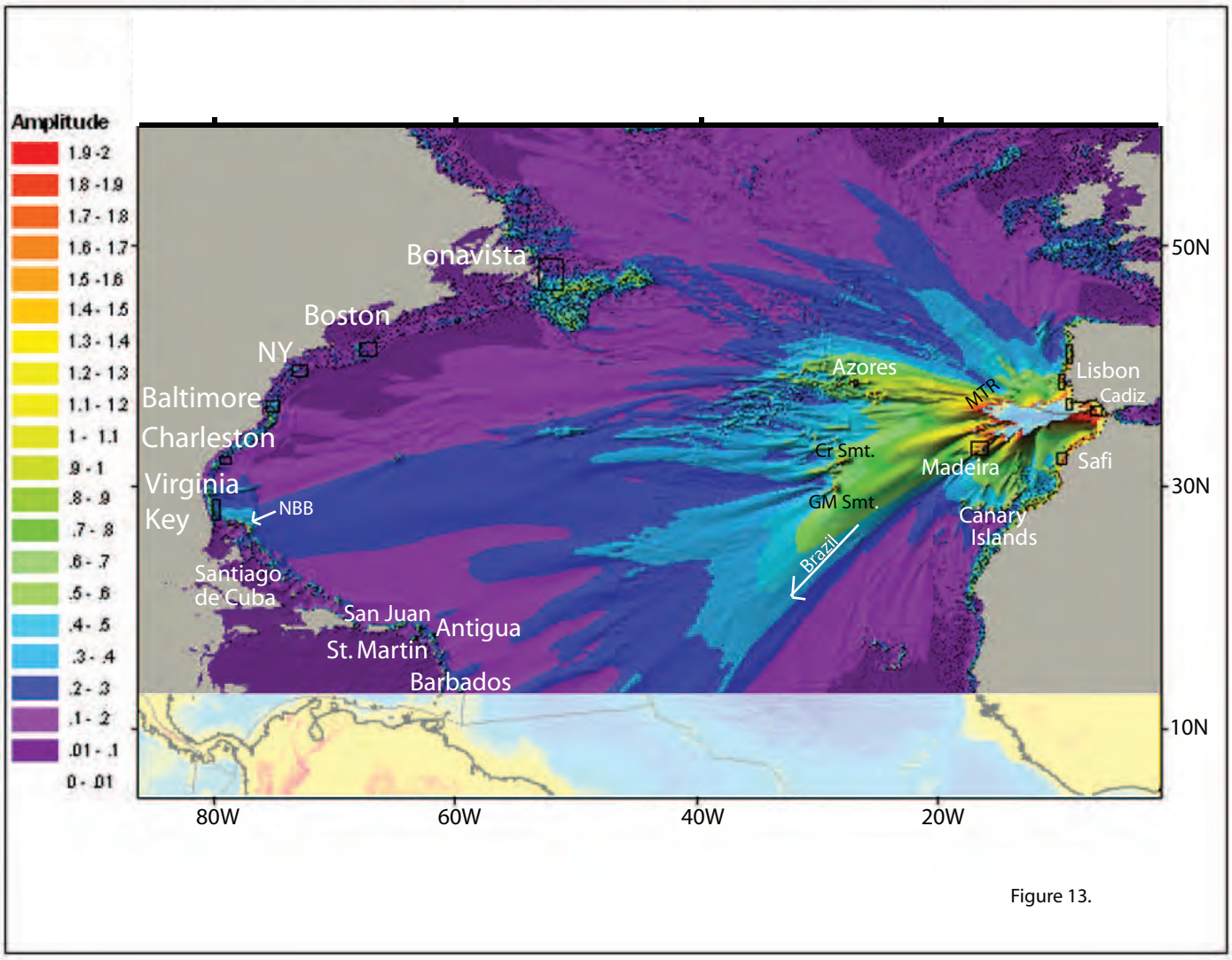

Figure 13.

Figure 14

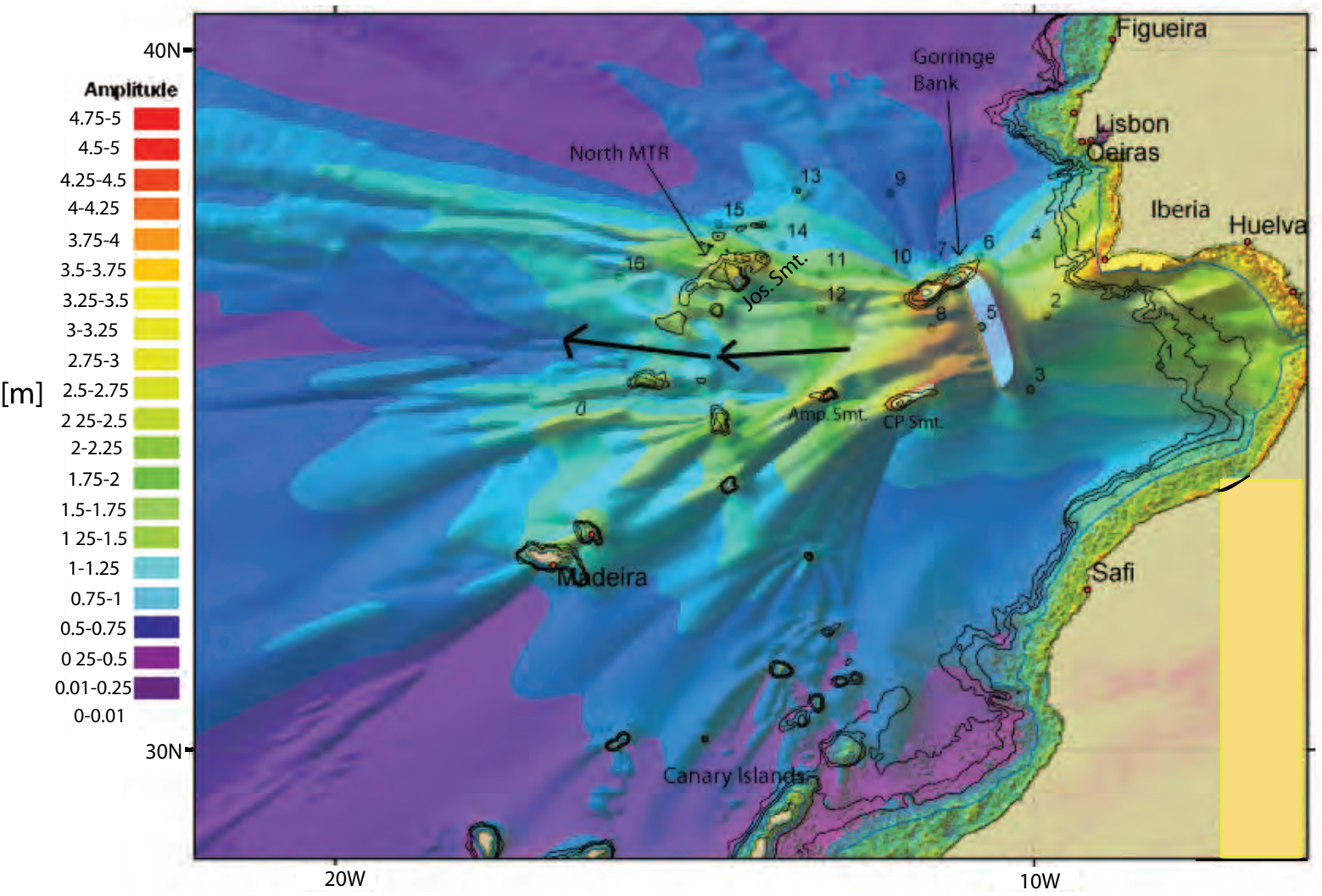

Figure 14.

Figure 15

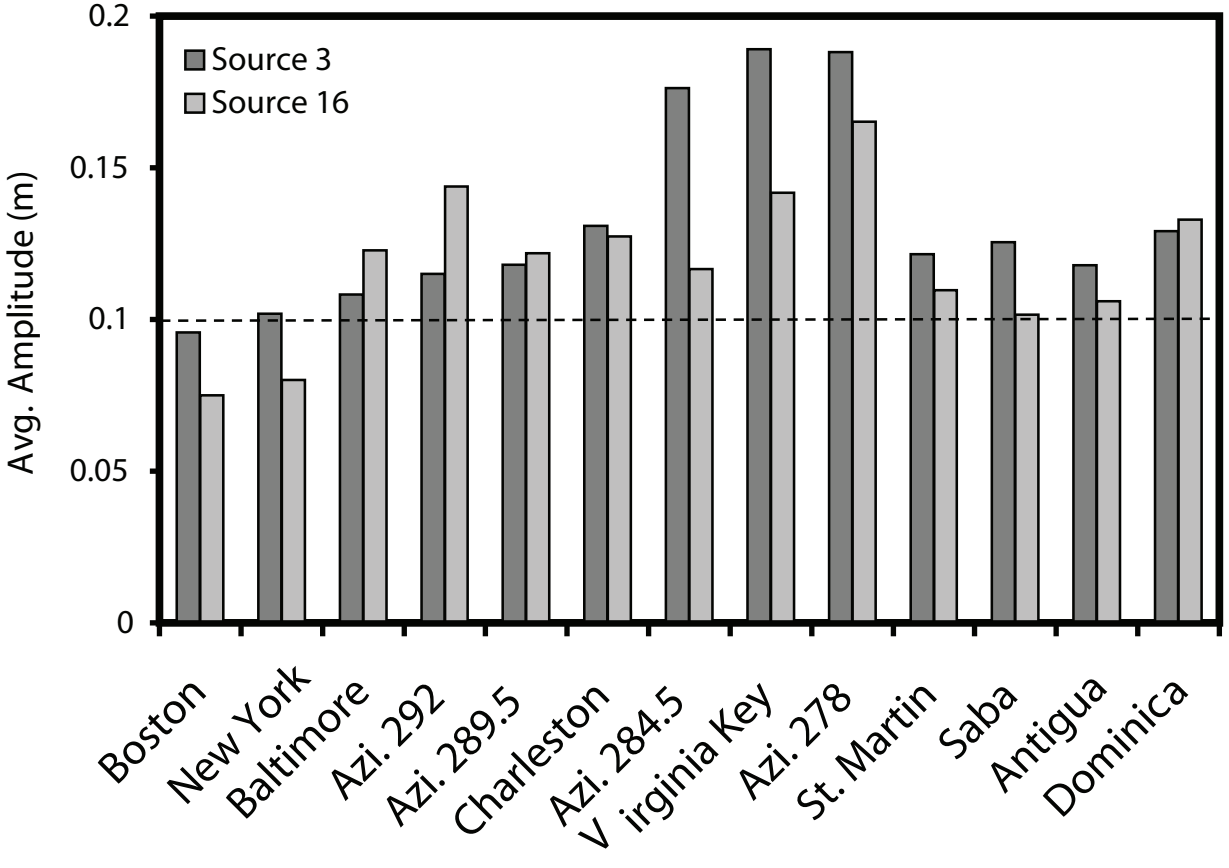
Source 3
Source 16
Avg. Amplitude (m)
0.2
0.15
0.1
0.05
0
Boston
New York
Baltimore
Azi. 292
Azi. 289.5
Charleston
Azi. 284.5
V irginia Key
Azi. 278
St. Martin
Saba
Antigua
Dominica

Figure 16

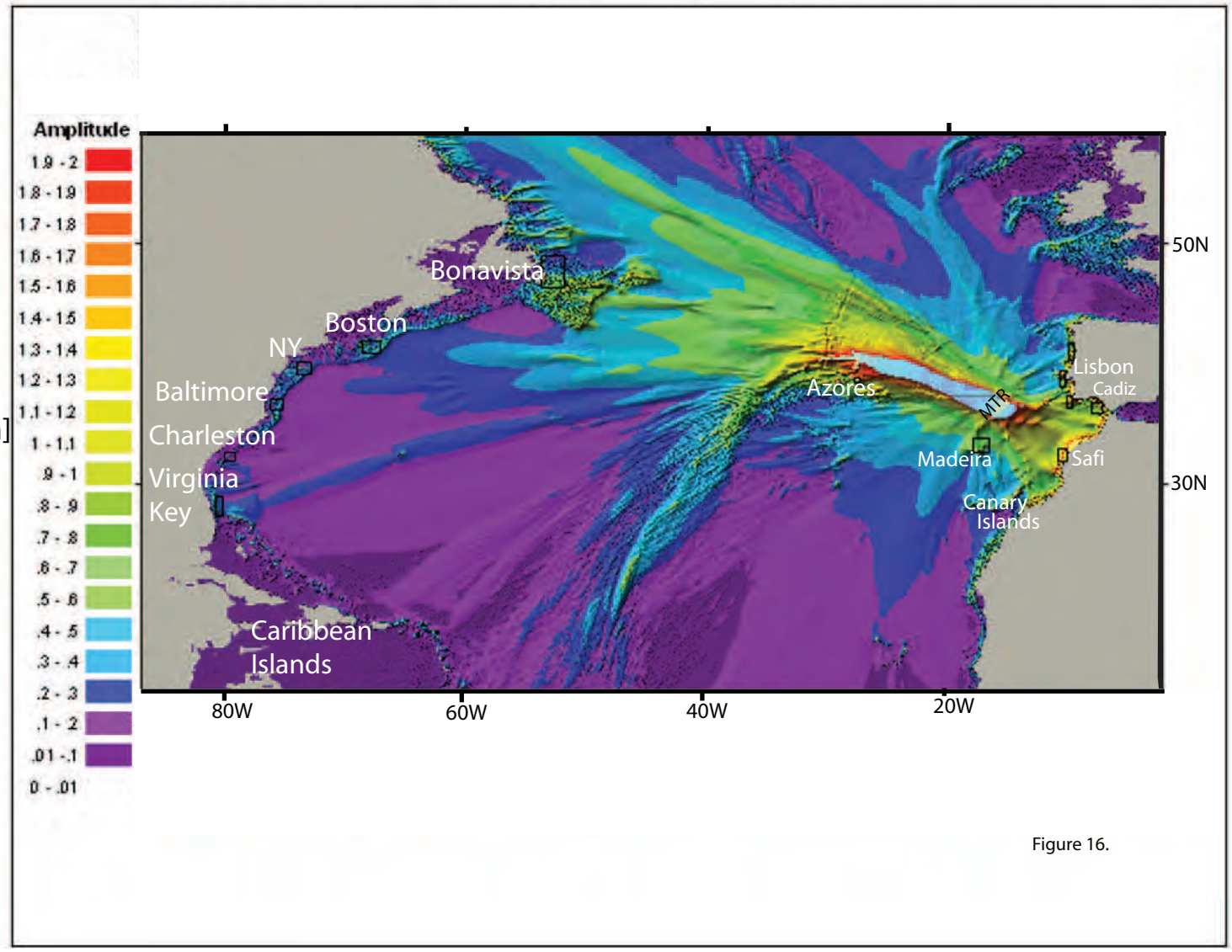

Figure 16.

Figure 17

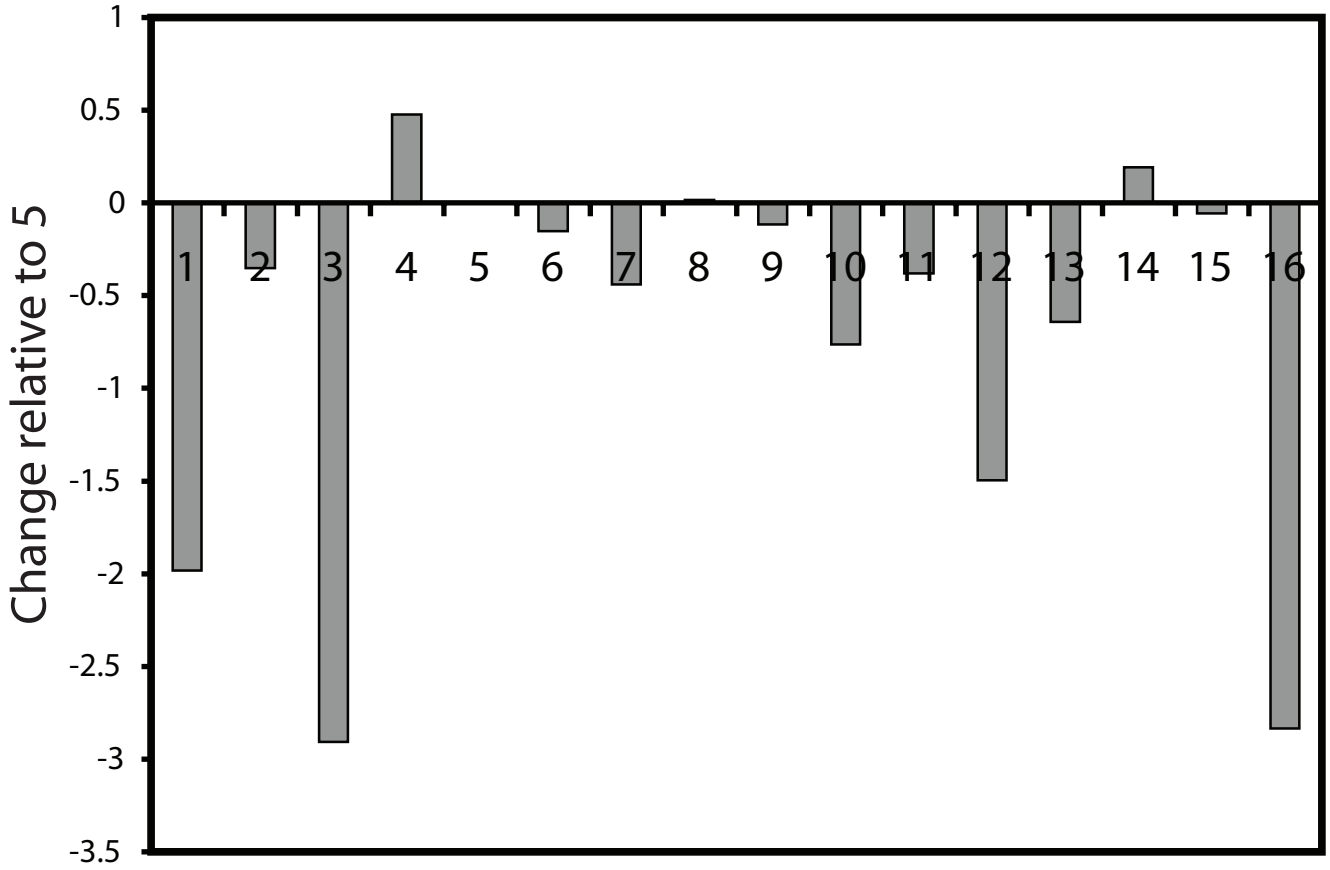
Change relative to 5
1
0.5
0
-0.5
-1
-1.5
-2
-2.5
-3
-3.5
1
2
3
4
5
6
7
8
9
10
11
12
13
14
15
16